Dalton Transactions

Accepted Manuscript

ROYAL SOCIETY OF CHEMISTRY

www.rsc.org/dalton

Targeting of DNA molecules, BSA/*c*-Met tyrosine kinase receptor and anti-proliferative activity of bis(terpyridine)copper(II) complexes

Dharmasivam Mahendiran[a], Raju Senthil Kumar[b], Vijayan Viswanathan[c], Devadasan Velmurugan[c] and Aziz Kalilur Rahiman[*a]

[a]*Post-Graduate and Research Department of Chemistry, The New College (Autonomous), Chennai 600 014, India.*

[b]*Department of Pharmaceutical Chemistry, Swami Vivekanandha College of Pharmacy, Elayampalayam, Tiruchengodu 637 205, India.*

[c]*CAS in Crystallography and Biophysics, University of Madras, Guindy Campus, Chennai 600 025, India.*

Abstract

A series of homoleptic bis(terpyridine)copper(II) complexes of the type $[Cu(L^{1-5})_2]Cl_2$ (**1–5**), where L^{1-5} = 4'-(4-substituted)-2,2':6',2''-terpyridines have been synthesized and characterized. The molecular structure of the complex **2** was confirmed by single crystal XRD technique, and the geometry of the complexes are best described as distorted octahedral. Structural parameters from the crystallographic and DFT studies are in good agreement with each other. The small HOMO–LUMO energy gap supports bioefficacy of the complexes. DNA binding studies show high intrinsic binding constant values 1.53 ± 0.15, 1.62 ± 0.08 and 3.09 ± 0.12 × 10^5 M^{-1} for complexes **1**, **2** and **3**, respectively with intercalative mode of binding to CT–DNA. The binding results were further supported by molecular docking studies. The experimental results indicate that the interaction between the complexes and BSA protein involves a static quenching mechanism. The molecular docking studies with *c*-Met tyrosine kinase receptor shows hydrophobic and π-π interactions. All the complexes bring about hydroxyl radical mediated DNA cleavage in the presence of H_2O_2. *In vitro* cytotoxicity of the complexes (**1**–**3**) were tested against three cancerous cells such as human breast adenocarcinoma (MCF-7), epithelioma (Hep-2) and cervical (HeLa) cell lines, and one nontumorigenic human dermal fibroblasts (NHDF) cell line by MTT reduction assay.

The morphological assessment data obtained by using Hoechst 33258 staining revealed that the complex **3** induce apoptosis much more effectively than the other complexes.

Keywords: Homoleptic complexes; DFT calculations; DNA interaction; Protein kinase receptor; Anti-proliferation.

*Corresponding author. Tel.: +91 44 2835 0297; Fax: +91 44 2835 2883.
E-mail address: akrahmanjkr@gmail.com

Introduction

DNA binding and cleavage are two critical events for gene mutation and carcinogenesis in biological systems.[1] Therefore, DNA targeting reagents may have great prospects as artificial nucleases, DNA structural probes or gene selective drugs.[2] Understanding the features that contribute to enhance DNA binding by small ligands or metal complexes is crucial for the development of drugs targeted to DNA. Metal ions play important roles in life process by serving as essential cofactors, fulfilling cellular functions that cannot met by organic molecules. Also, metal ions have been frequently incorporated into pharmaceuticals for diagnostic or therapeutic purposes.[3–5] Many properties of metal complexes such as size, oxidation state, geometry and chirality could influence the binding mode to DNA. Moreover, inorganic complexes offer an advantage for studying the role that molecular design and geometry play in binding with DNA because of their relative ease in preparation and modification.[6] Additionally, the metal could probably act as a carrier and stabilizer for the drug ligands until it reaches its target. At the same time, the organic drug ligands could protect the metal and prevent side reactions in its transit toward a second target of biological action. Therefore, the combined effects between the metal and the ligands could result in enhancement of biological activities or activate new action mechanisms. In the

search for new chemotherapeutic agents, inorganic complexes that function by intercalation of their aromatic ligands into the base pairs of DNA are of intense interest.[7]

Medicinal inorganic chemistry has been greatly influenced by the clinical successes of cisplatin and other platinum-based drugs in cancer therapy.[8] However, the use of platinoid compounds has often been limited due to their severe side effects and drug resistance.[9,10] Such limitations of cisplatin have motivated extensive investigation into alternative metal based anticancer agents. Thus, the compounds based on metals other than platinum have been postulated and are under study to complement the anticancer drugs currently in clinical use. Among these, the copper(II) complexes are considered the best alternatives to cisplatin because of their bio-friendly nature as copper plays a significant role in biological systems, and it has been demonstrated that copper accumulates in tumors due to the selective permeability of cancer cell membranes. A great majority of copper(II) complexes currently studied in the anticancer research field exert their anti-proliferative activities through ligand exchange. Thus, a number of copper complexes have been screened for anticancer activity, and some of them were found to be active both *in vitro* and *in vivo*,[11–13] and its complexes are able to promote the generation of reactive oxygen species (ROS), which has been exploited to oxidatively break the DNA strands and further to inhibit the proliferation of tumor cells.[14–16]

Substituted-2,2':6',2"–terpyridine ligands have attracted widespread attention due to their ability to form complexes with transition metals, and applications in various fields such as supramolecular chemistry, asymmetric catalysis, photosensitization and antitumor chemo-therapeutics.[17–19] The terpyridine complexes are well documented for their high DNA affinity through intercalation, DNA nuclease activity and cytotoxicity.[20–22] A variety of copper complexes have been designed for the above said reasons[23,24] and several copper(II) terpyridine complexes have shown considerable nuclease and antitumor activity in physiologically relevant conditions.[25–27] Among them, the bis(terpyridine) complexes bind

strongly to DNA and exhibit prominent anticancer activities by inducing cell death.[28–32] To the best of our knowledge, the effect of substituents and DFT studies of such homoleptic copper(II) complexes are scare in literature.

In view of all these observations, and in continuation of our recent report on heteroleptic copper(II) complexes with terpyridines and naproxen drug,[33] we have been interested in exploring the theoretical and biological properties of bis(4′-(4-substituted)-2,2′:6′,2″–terpyridine)copper(II) complexes. A host of methods like absorption, emission, circular dichroism, viscosity, cyclic voltammetry and electrophoresis techniques have been used to probe the DNA interaction of the synthesized copper(II) complexes. The experimental BSA binding studies was investigated by using UV-Vis and fluorescence spectroscopic techniques. The DNA molecular docking studies was performed by using AutoDock Tools (ADT) version 1.5.6 and AutoDock version 4.2.5.1 docking programmes and BSA docking studies was carried out by using Schrödinger software. The cytotoxicity of the complexes was tested against three cancerous and one non-cancerous cell lines using MTT assay. The morphological assessment has been studied by Hoechst 33258 staining method. Further, an in-depth theoretical understanding of the geometries on DFT and HOMO-LUMO analysis was performed in order to elucidate information regarding electrophilicity (ω), hardness (η), chemical potential (μ) and nucleus independent chemical shift (NICS) calculations using the Gaussian 03 program.

Experimental

Materials

2-Acetyl pyridine, 4-methylbenzaldehyde, 4-methoxybenzaldehyde, 3,4-dimethoxy benzaldehyde, 2-furfuraldehyde and thiophene-2-carboxaldehyde used for ligand synthesis were purchased from AVRA chemicals (India). Solvents of analytical grade were purchased from E. Merck, and used as received without further purification. Tetra(*n*-butyl)ammonium

perchlorate (TBAP) used as the supporting electrolyte in the electrochemical measurements was purchased from Fluka (Switzerland). Agarose (molecular biology grade) and ethidium bromide were procured from Sigma-Aldrich (USA). Calf-thymus DNA (CT–DNA) and supercoiled pBR322 DNA were purchased from Bangalore Genei (India). Tris(hydroxymethyl)aminomethane-hydrochloride (Tris-HCl) buffer (pH, 7.3) was used for all DNA binding and cleavage studies.

Physical measurements

The elemental analysis (CHN) of the compounds was carried out with a Carlo Erba model-1106 elemental analyzer. IR spectra were recorded on a Perkin-Elmer FT IR 8300 model spectrophotometer using KBr disc technique in the range of 4000–400 cm^{-1}. Electronic absorption spectra were recorded using Perkin-Elmer Lambda-35 spectrophotometer in the range of 200–800 nm. Fluorescence spectra were recorded on a Horiba Jobin Yvon FluoroLog SPEX-F311 spectrofluorometer. Circular dichroic spectra were recorded in the spectral region of 200−300 nm with a Jasco J-815 spectropolarimeter at 25 °C using 0.1 cm path quartz cell. Electrospray ionization (ESI) mass spectra were recorded on Q-Tof mass spectrometer using acetonitrile as a carrier solvent. Thermogravimetric analysis was carried out using SDT Q600 US analyzer (ASTM E1131) to record simultaneously TGA/DTG curves under a nitrogen atmosphere with a heating rate of 20 °C/min in the temperature range from 25 °C to 900 °C. Cyclic voltammograms were obtained on CHI 602D (CH Instruments Co., USA) electrochemical analyzer. The electrochemical workstation was equipped with a three electrode system, namely, glassy carbon, platinum wire and Ag/AgCl as working, auxiliary and reference electrodes, respectively. Tetra(*n*-butyl)ammonium perchlorate (TBAP) was used as supporting electrolyte for the electrochemical work and nitrogen gas was purged prior to all the measurements.

The ligands 4'-(4-tolyl)-2,2':6',2"-terpyridine (L^1), 4'-(4-methoxyphenyl)-2,2':6',2"-terpyridine (L^2), 4'-(3,4-dimethoxyphenyl)-2,2':6',2"-terpyridine (L^3), 4'-(furan-2-yl)-2,2':6',2"-terpyridine (L^4) and 4'-(thiophen-2-yl)-2,2':6',2"-terpyridine (L^5) were synthesized by following the procedure describe in the literature.[34]

General procedure for synthesis of homoleptic copper(II) complexes (1–5)

A hot methanolic solution of 4′-(4-substituted)-2,2′:6′,2′′-terpyridine ($L^{1–5}$, 1 mmol) was added slowly with constant stirring to a hot methanolic solution of $CuCl_2.2H_2O$ (0.09 g, 0.5 mmol), and the resulting solution was refluxed for 2 h. After cooling the reaction mixture to room temperature, the resulting solid product was collected by filtration, washed with diethyl ether, dried under vacuum, and recrystallized from methanol.

$[Cu(L^1)_2]Cl_2$ (1)

Yield: 0.72 g, (92.3%); Colour: Green; Anal. Calc. for: $C_{44}H_{34}N_6Cl_2Cu$ (781.23): C, 67.65; H, 4.39; N, 10.26; Found: C, 68.37; H, 4.53; N, 10.01%. Selected IR data (KBr, υ/cm^{-1}): 1636 υ(C=N), 1552 υ(C=C), 511 υ(M–N). UV-Vis (DMF): [λ_{max} (nm) (ε, $dm^3\ mol^{-1}\ cm^{-1}$)]: 287 (40,400), 338 (11,640), 716 (160). ESI–MS (m/z): 710.33 $[Cu(L^1)_2]^+$. Conductance (Λ_M, $\Omega^{-1}\ cm^2\ mol^{-1}$) in DMF: 152. $g_{\|} = 2.11$, $g_{\perp} = 2.01$. $\mu_{eff} = 1.78$ BM.

$[Cu(L^2)_2]Cl_2$ (2)

Yield: 0.75 g, (92.5%); Colour: Green; Anal. Calc. for: $C_{44}H_{34}N_6O_2Cl_2Cu$ (813.23): C, 64.98; H, 4.21; N, 10.33; Found: C, 64.41; H, 4.53; N, 10.12%. Selected IR data (KBr, υ/cm^{-1}): 1638 υ(C=N), 1559 υ(C=C), 496 υ(M–N). UV-Vis (DMF): [λ_{max} (nm) (ε, $dm^3\ mol^{-1}\ cm^{-1}$)] 285 (39,440), 337 (11,00), 747 (244). ESI–MS (m/z): 742.33 $[Cu(L^2)_2]^+$. Conductance (Λ_M, $\Omega^{-1}\ cm^2\ mol^{-1}$) in DMF: 149. $g_{\|} = 2.13$, $g_{\perp} = 2.06$. $\mu_{eff} = 1.76$ BM.

$[Cu(L^3)_2]Cl_2$ (3)

Yield: 0.81 g, (93.1%); Colour: Green; Anal. Calc. for: $C_{46}H_{38}N_6O_4Cl_2Cu$ (873.28) C, 63.27; H, 4.39; N, 9.62; Found: C, 62.35; H, 4.60; N, 9.44%. Selected IR data (KBr, υ/cm^{-1}): 1642 υ(C=N), 1558 υ(C=C), 492 υ(M–N). UV-Vis (DMF): [λ_{max} (nm) (ε, dm^3 mol^{-1} cm^{-1})]: 286 (35,040), 327 (10,600), 743 (208). ESI–MS (m/z): 802.38 $[Cu(L^3)_2]^+$. Conductance (Λ_M, Ω^{-1} cm^2 mol^{-1}) in DMF: 154. $g_{\|} = 2.15$, $g_{\perp} = 2.09$. $\mu_{eff} = 1.82$ BM.

$[Cu(L^4)_2]Cl_2$ (4)

Yield: 0.68 g, (93.0%); Colour: Green; Anal. Calc. for: $C_{38}H_{26}N_6O_2Cl_2Cu$ (733.10) C, 62.26; H, 3.57; N, 11.46; Found: C, 62.62; H, 4.17; N, 10.98%. Selected IR data (KBr, υ/cm^{-1}): 1640 υ(C=N), 1569 υ(C=C), 486 υ(M–N). UV-Vis (DMF): [λ_{max} (nm) (ε, dm^3 mol^{-1} cm^{-1})]: 271 (42,400), 330 (12,200), 742 (320). ESI–MS (m/z): 662.20 $[Cu(L^4)_2]^+$. Conductance (Λ_M, Ω^{-1} cm^2 mol^{-1}) in DMF: 156. $g_{\|} = 2.14$, $g_{\perp} = 2.02$. $\mu_{eff} = 1.83$ BM.

$[Cu(L^5)_2]Cl_2$ (5)

Yield: 0.68 g, (93.4%); Colour: Green; Anal. Calc. for: $C_{38}H_{26}N_6S_2Cl_2Cu$ (765.24): C, 59.64; H, 3.42; N, 10.98; Found: C, 60.57; H, 3.69; N, 10.03%. Selected IR data (KBr, υ/cm^{-1}): 1648 υ(C=N), 1561 υ(C=C), 480 υ(M–N). UV-Vis (DMF): [λ_{max} (nm) (ε, dm^3 mol^{-1} cm^{-1})]: 283 (36,320), 329 (11,440), 720 (128). ESI–MS (m/z): 694.33 $[Cu(L^5)_2]^+$. Conductance (Λ_M, Ω^{-1} cm^2 mol^{-1}) in DMF: 155. $g_{\|} = 2.16$, $g_{\perp} = 2.08$. $\mu_{eff} = 1.88$ BM.

Crystal structure determination

Single crystals of complex **2** were grown by slow evaporation from methanol. A single crystal with dimension of 0.30 × 0.25 × 0.20 mm was mounted on glass fibre with epoxy cement for diffraction experiment. All geometric and intensity data were collected using an automated Bruker SMART APEX CCD diffractometer equipped with a fine focus 1.75 kW sealed tube, Mo-Kα X-ray source (λ = 0.71073 Å) with increasing ω (width of 0.3° per frame) at a scan speed of 5 sec per frame. The intensity data were corrected for the

Lorentz polarization as well as for absorption effects. The crystal structure was solved by direct methods using SHELXS-2014/7 and refined by full-matrix least-squares using SHELXL-2014/7.[35]

Computational details

Gaussian 03[36] software package was used for theoretical calculation. The quantum chemical calculations were performed applying DFT method with Becke-3-Lee-Yang-Parr (B3LYP) supplemented with the standard 6-31G(d) and LANL2DZ basis set.[37] The optimized geometry corresponding to the minimum on the potential energy surface has been obtained by solving self-consistent field equation iteratively.

DNA binding studies

Absorption spectral titration

Electronic absorption spectroscopy is employed to examine the binding mode of CT–DNA with small molecules. The UV absorbance of CT–DNA at 260 and 280 nm in 5 mM Tris-HCl/50 mM NaCl buffer (pH, 7.3) solution at room temperature gave a ratio of 1.8–1.9:1, indicating that the DNA was sufficiently free from proteins.[38] Stock solutions of CT–DNA was prepared in Tris-HCl/NaCl buffer and stored at 4 ºC for less than 4 days. The concentration of DNA in nucleotide phosphate was determined by UV absorbance at 260 nm. The molar absorption coefficient of CT–DNA was taken as 6600 $M^{-1}cm^{-1}$. Absorption titration experiments were performed by maintaining the constant complex concentration (25 μM) and varying the concentration of CT–DNA (0−5.0 μM). Complex-DNA solutions were allowed to incubate for 30 min at room temperature before measurements were taken. While measuring the absorption spectra, equal quantity of CT–DNA was added to both the complex solution and reference solution to eliminate the absorbance of CT–DNA itself. The intrinsic binding constants K_b, can be obtained by the following equation:

$$[DNA]/(\varepsilon_a - \varepsilon_f) = [DNA]/(\varepsilon_b - \varepsilon_f) + 1/K_b\,(\varepsilon_b - \varepsilon_f)$$

where ε_a, ε_f, and ε_b correspond to A_{obs}/[complex], the extinction coefficient for the free copper complex, and the extinction coefficient for the copper complex in the fully bound form, respectively. A plot of [DNA]/($\varepsilon_a - \varepsilon_f$) *versus* [DNA] gives K_b as the ratio of the slope to the intercept.

DNA melting experiments

DNA melting experiments were carried out by monitoring the absorption (260 nm) of CT–DNA (100 μM) at various temperatures in the absence and presence of complexes (25 μM). The melting temperature T_m was calculated by plotting temperature *versus* relative absorption intensity (A/A_0), and measurements were carried out using a Perkin–Elmer Lambda 35 spectrophotometer equipped with a Peltier temperature controlling programmer (PTP 6) (±0.1 °C) on increasing the temperature of the solution by 0.5 °C per min.

Ethidium bromide displacement studies

DNA binding studies using fluorescence spectra was carried out by employing the procedure reported by us previously.[39]

Circular dichroic spectral studies

Circular dichroic spectra were recorded in the range 200–300 nm. The concentration of CT–DNA (100 μM) was kept constant and the concentration of the complex varied from 10 to 20 μM. The sample solution was mixed and incubated at room temperature before measurments.

Viscosity measurements

Viscometric experiments were carried out using an Ostwald-type viscometer of 2 mL capacity, thermostated in a water bath maintained at 25 ± 1 ºC. The desired concentrations of DNA (20 μM) and complexes (0–100 μM) were prepared by using Tris-HCl/NaCl buffer (pH = 7.3). Mixing of the solution was achieved by purging nitrogen gas through viscometer. The flow times were measured with a digital timer, and each sample was measured three times for

accuracy, and an average flow time was calculated. Data are presented as η/η_0 *vs*. 1/R, where η is the relative viscosity of DNA in the presence of the copper(II) complex and η_0 is the relative viscosity of DNA alone. The viscosity values were calculated from the observed flow time of the solutions containing DNA (t) and corrected for that of the buffer alone (t_b), using the following equation:[40]

$$\eta = (t - t_b)/t_b$$

Electrochemical titration

The electrochemical investigation of metal-DNA interaction may be a useful supplement to spectroscopic methods and provide information about interaction with both the reduced and oxidized form of the metal. Double distilled water was used to prepare the buffer solutions. The solutions of complexes and DNA were prepared by using DMF and Tris-HCl/NaCl buffer (pH 7.3), respectively. The concentration of complexes can be taken as 100 μM and also for DNA. Solutions were deoxygenated by purging with N_2 gas prior to measurements.

Molecular docking studies

Molecular docking studies were carried out using the AutoDock Tools (ADT) version 1.5.6 and AutoDock version 4.2.5.1 docking programmes. Structures of the complexes (**1**–**3**) were converted into PDB format from mol format by OPENBABEL. The crystal structure of the B-DNA dodecamer d(CGCGAATTCGCG)$_2$ (PDB ID: 1BNA) was downloaded from the protein data bank (http://www.rcsb.org./pdb). Receptor (DNA) and ligand (complexes) files were prepared using AutoDock Tools. First, all the heteroatoms including water molecules were deleted and polar hydrogen atoms and Kollman charges were added to receptor molecule, then rotatable bonds in ligands were assigned. All other bonds were allowed to rotatable. The DNA was enclosed in a box with number of grid points in x × y × z directions, 60 × 60 × 110 and a grid spacing of 0.375 Å. Lamarckian genetic algorithm, as implemented

in AutoDock, were employed to perform docking calculations. All other parameters were default settings. For each of the docking cases, the lowest energy docked conformation, according to the Autodock scoring function, was selected as the binding mode. Visualization of the docked position has been done by using PyMOL molecular graphics programs.

BSA binding studies

Interaction of the bis(terpyridine)copper(II) complexes with BSA was carried out by UV-Vis and fluorescence spectral techniques. UV-Vis measurements of BSA in the absence and presence of copper(II) complexes (**1**−**5**) were made in a range of 200−500 nm. BSA concentration was fixed at 10 μM. The influences of the absorbance of copper(II) complexes were eliminated by adding in the reference cells the solutions of copper(II) complexes of the same concentrations as in the sample solution.

The binding of copper(II) complex **3** with BSA was studied by using fluorescence spectra recorded at a fixed excitation wavelength of 280 nm and monitoring the emission at 348 nm. A fixed concentration of BSA (10 μM) was titrated by successive additions of the stock solution of the copper(II) complex (0–50 μM) at room temperature. Before measurements, the mixture was shaken up and incubated at room temperature for 30 min.

Molecular docking with *c*-Met kinase

The molecular docking with *c*-Met tyrosine kinase was carried out by employing the procedure reported by us previously.[39]

Gel electrophoresis

Cleavage of DNA by bis(terpyridine)copper(II) complexes (**1–3**) was monitored by determining their ability to convert supercoiled DNA (Form I) to open circular (Form II) and linear (Form III) forms using the agarose gel electrophoresis technique. In the cleavage experiments, the plasmid pBR322 DNA (33.3 μM) was treated with different concentration of complexes. The samples were incubated at 37 ºC for 1 h, a loading buffer containing 25%

bromophenol blue, 0.25% xylene cyanol and 30% glycerol was added, and electrophoresis was performed at 50 V for 1 h in TAE buffer using 0.8% agarose gel containing 1.0 mg/mL ethidium bromide, and was photographed on UVItec gel documentation system. The degree of DNA cleavage activity was expressed in terms of the percentage of conversion of the SC DNA to NC DNA according to the following equation:

$$\text{DNA cleavage activity (\%)} = \frac{(\%\ \text{of SC DNA})_{\text{control}} - (\%\ \text{of SC DNA})_{\text{sample}}}{(\%\ \text{of SC DNA})_{\text{control}}} \times 100$$

Cell proliferation assay

Cell lines

Human breast adenocarcinoma (MCF-7), epithelioma (Hep-2) and cervical (HeLa) cancer cell lines, and a nontumorigenic human dermal fibroblasts (NHDF) cell line were obtained from National Centre for Cell Science (NCCS), Pune, India, and cultured in Dulbecco's Modified Eagles Medium (DMEM) (St. Louis, Mo, USA), supplemented with 10% heat inactivated fetal bovine serum (FBS), penicillin 100 µg/mL, streptomycin 20 µg/mL, kanamycin acid sulphate 20 µg/mL and 7.5% sodium bicarbonate solution. The cell lines were maintained at 37 °C in a 5% CO_2 incubator and the media were changed frequently. MTT (3-(4,5-dimethyl-2-thiazolyl)-2,5-diphenyltetrazolium bromide) was obtained from Himedia, India.

MTT assay

The cytotoxic effect of complexes (**1–3**) on three cancerous cell lines such as human breast adenocarcinoma (MCF-7), epithelioma (Hep-2) and cervical (HeLa) and one nontumorigenic human dermal fibroblasts (NHDF) cell lines was determined by MTT assay as described by Mosmann.[41] The cells were grown in DMEM medium containing 10% FBS. For screening experiments, the cells (5×10^3 cells/well) were plated in 96-well plates with the medium containing 10% FBS and incubated for 24 h under CO_2 at 37 ºC. Later, the medium

was replaced with DMEM containing 1% FBS and the complexes **1**–**3** (100, 50, 25, 10, 5 and 2 μM) dissolved in 0.1% DMSO was added to the cells incubated at 37 ºC in 5% CO_2. After treatment, the plates were incubated for 24 h and 10 μL of MTT prepared at a concentration of 5 mg/mL was added to each well and incubated for 4 h. Purple color farmazone crystals formed were then dissolved in 100 μL of dimethylsulfoxide (DMSO). Viability of the cells was determined by measuring the absorbance at 570 nm in a multi well ELISA plate reader. The absorbance at 570 nm was also measured for wells without any sample as blank. The % of cell viability was evaluated using the following equation:

$$\text{Cell viability (\%)} = \frac{A_{570\ \text{nm}} \text{ of treated cells}}{A_{570\ \text{nm}} \text{ of control cells}} \times 100$$

Hoechst staining and photomicroscopy

The morphology of MCF-7 cells after treatment was analyzed with the aid of Hoechst 33258 staining. First, MCF-7 cells (1×10^5) were seeded into 96-well plate in 2 mL of medium for 48 h. Then, varying amounts of complexes (**1**–**3**) were added to each plate, and incubated for 48 h. After 48 h, the cells were washed in phosphate-buffered saline (PBS) and stained for 10 min at room temperature in PBS containing 40% paraformaldehyde and 10 mg/mL Hoechst 33258. The MCF-7 cells for Hoechst staining were grown on sterilized cover slips and processed as described with modifications.[42] Briefly, after washing one time with PBS, cells were fixed with 3.7% formaldehyde in PBS for 10 min, washed one time with PBS, stained with 0.4 mg/mL Hoechst (Molecular Probes, Eugene, USA) in PBS for 15 min, washed two times with PBS, and then one time with water. Cover slips were then air-dried and mounted with Slow Fade (Molecular Probes) mounting media. Morphological evaluations of nuclear condensation and fragmentation were performed immediately after staining by means of fluorescent microscope (Olympus, Japan) at 550 nm of emission.

Results and discussion

Synthesis of bis(terpyridine)copper(II) complexes

The homoleptic bis(terpyridine)copper(II) complexes (**1**–**5**) were obtained in good yields and sufficiently pure forms by the reaction of copper(II) chloride (0.5 mmol) and the respective terpyridine ligands (1 mmol) in methanol (**Scheme 1**). The authenticities of the complexes were ascertained by elemental analysis, FT IR, UV-Vis and ESI-MS spectral methods along with single crystal XRD.

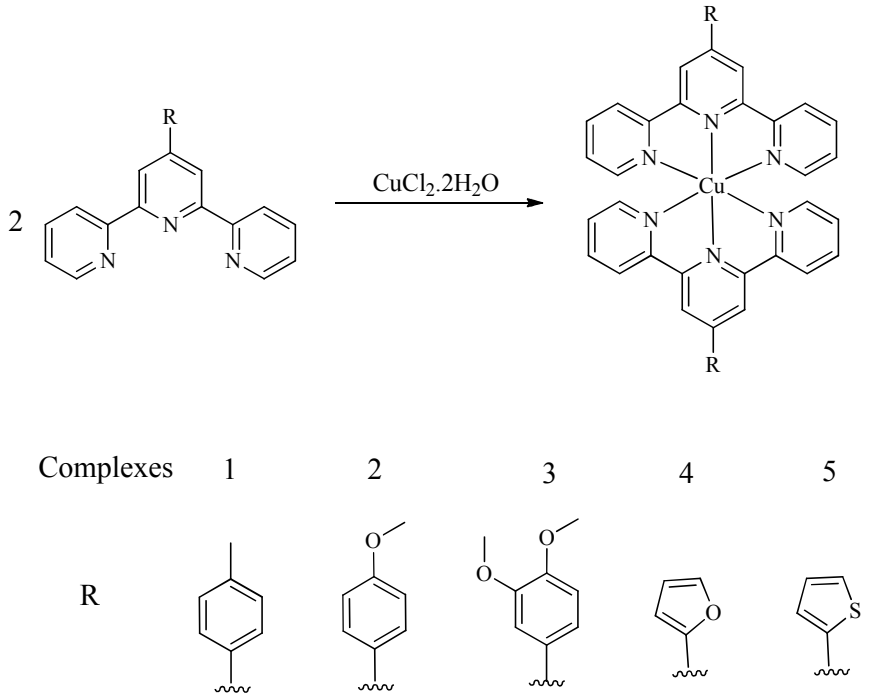

Scheme 1 Synthesis of homoleptic bis(terpyridine)copper(II) complexes (**1**–**5**).

The IR spectral signatures of the ligands show characteristic bands in the range of 1648–1670 and 1570–1579 cm^{-1} assigned to υ(C=N) and υ(C=C) stretching vibrations, respectively. For the metal complexes, although no appreciable shifts in the vibrations attributed to aromatic and υ(C=C) of the terpyridines were observed, absorption due to υ(C=N) shift to lower frequency (28–52 cm^{-1}) after complexation. This indicates the participation of nitrogen of terpyridines in the coordination. Moreover, the bands in the low

wave number region of 480–511 cm^{-1} were assigned to υ(M–N). The ESI mass spectra of the complexes were recorded to establish their stoichiometric composition. **Fig. S1** depicts the mass spectrum of complex **2** that shows molecular ion peak at *m*/*z* 742 due to $[Cu(L^2)_2]^+$, which is equivalent to its molecular weight excluding the counter ions. The base peak at *m*/*z* 402 corresponds to $[Cu(L^2)]^+$. The mass spectral results are in good agreement with the proposed molecular formulae of the complexes.

The diffuse reflectance spectroscopy has been used to estimate the width of the energy gap using Kubelka–Munk (K–M) model.[43] A graph is plotted between $[F(R)h\upsilon]^2$ and hυ, the intercept value is the band gap energy (**Fig. S2**). The solid state reflectance spectra of complexes **1** and **2** show broad absorption band at 281, 283 nm (4.41, 4.56 eV) with a small band at 758 and 747 nm (1.63, 1.65 eV), respectively, and the liquid UV-Vis absorption spectra of complexes **1** and **2** exhibit band gap values of 4.35, 1.65 eV (285, 749 nm) and 4.32, 1.66 eV (287, 743 nm), respectively. The similar pattern obtained in UV-Vis spectra of the complexes in solid and solution implies that the octahedral geometries of complexes, as evidenced by the X-ray crystal structure of complex **2**, is retained in solution.

3.2. Structural description of $[Cu(L^2)_2]Cl_2$ (2)

Suitable single crystals of green coloured copper(II) complex **2** was obtained by slow evaporation of the reaction mixture for several days, which crystallizes as **2**·CH_3OH·$(H_2O)_6$. The complex **2** crystallized in trigonal crystal system and *"$P3_221$"* space group, the unit cell dimensions are a = 16.0226(4), b = 16.0226(4), c = 34.0974(12) Å, and α = 90°, β = 90° and γ = 120°. The crystal data and structure refinement parameters are listed in **Table 1**, while the selected bond lengths and bond angles are listed in **Table S1**. The ORTEP diagram with 50% thermal ellipsoids of molecule is shown in **Fig. 1**. The complex crystallized with eight isolated atoms, two chloride ions, six oxygen atoms along with one lattice methanol molecule. The crystal structure of the complex **2** shows the central Cu^{2+} ion bonding with six

nitrogen and form a octahedral coordination geometry. The octahedral geometry was formed by the bonding of central Cu^{2+} ion with three nitrogen atoms (N1, N2 and N3) of one molecule of terpyridine ligand and three nitrogen atoms (N4, N5 and N6) of another molecule of terpyridine ligand. The bond distance of Cu–N1, Cu–N2, Cu–N3, Cu–N4, Cu–N5 and Cu–N6 are 2.235(7), 1.975(7), 2.212(8), 2.110(7), 1.954(7) and 2.127(8) Å, respectively. The terpyridine rings bonding to the other terpyridine rings with carbon-carbon interaction. The bond distance of C5–C6, C10–C11, C27–C28 and C32–C33 are 1.498(2) Å, 1.493(2) Å, 1.480(1) Å and 1.458(2) Å, respectively. The carbon atom of each pyridine ring of terpyridine bonding with carbon atom of other pyridine ring, and it will makes a five membered rings with copper atom [Cu–N1–C5–C6–N2], [Cu–N2–C10–C11–N3], [Cu–N4–C27–C28–N5] and [Cu–N5–C32–C33–N6]. In this structure, half of the ligand of N2 atom and other half of the ligand of N5 atom attached to the copper is almost planar, which is evidenced from the bond angle N2–Cu– N5 = 178.6(4)°.

Non-covalent (like π-stacking) interactions with aryl hydrogen and hydrogen bonding network are important class in supramolecular chemistry and crystal engineering. The molecular packing in the crystalline solid is constituted by intramolecular and intermolecular hydrogen bonds and the hydrogen bonding parameters are listed in **Table S2**. The crystal packing is stabilized by C–H···O and C–H···Cl types of inter molecular interaction and C–H···Cl intramolecular interaction in addition to van der Waals forces. In the intermolecular interaction C23–H23···O2 hydrogen bonds forming a chain C(12) running along "c" axis as shown in **Fig. 2**. In the crystal, the two molecules are also held together by C–H···π interactions between the H(22C) atoms and centroids of pyridine ring [N(1)–C(1)–C(2)–C(3)–C(4)–C(5)] with distance of 3.766(17) Å and the corresponding symmetry code is Cg1: –1–x,–x+y,2/3–z as shown in **Fig. S3**.

In addition to the single crystal X-ray studies, in order to substantiate the presence of solvent molecules, the thermal properties of the complex **2**·CH_3OH·$(H_2O)_6$ was also carried out by thermogravimetric (TG) and differential thermal (DTA) analysis (**Fig. 3**). The thermal decomposition of this complex takes place with two main weight loss steps. First weight loss starting from 72 to 124 °C with an exothermic peak in the DTG curve at 77 °C, which is attributed to the release of one lattice methanol and six lattice water molecules (obs. 13.31%, cal. 14.68%). The second weight loss starting from 276 to 392 °C with an exothermic peak in the DTG curve at 357 °C can be attributed to the losses of Cu(atpy) and two lattice chlorine atom (obs. 50.43%, cal. 49.70%). Similar observations have been reported in the literature.[44,45] The observed data strongly supports the presence of lattice molecules in the single crystal structure of complex **2**·CH_3OH·$(H_2O)_6$.

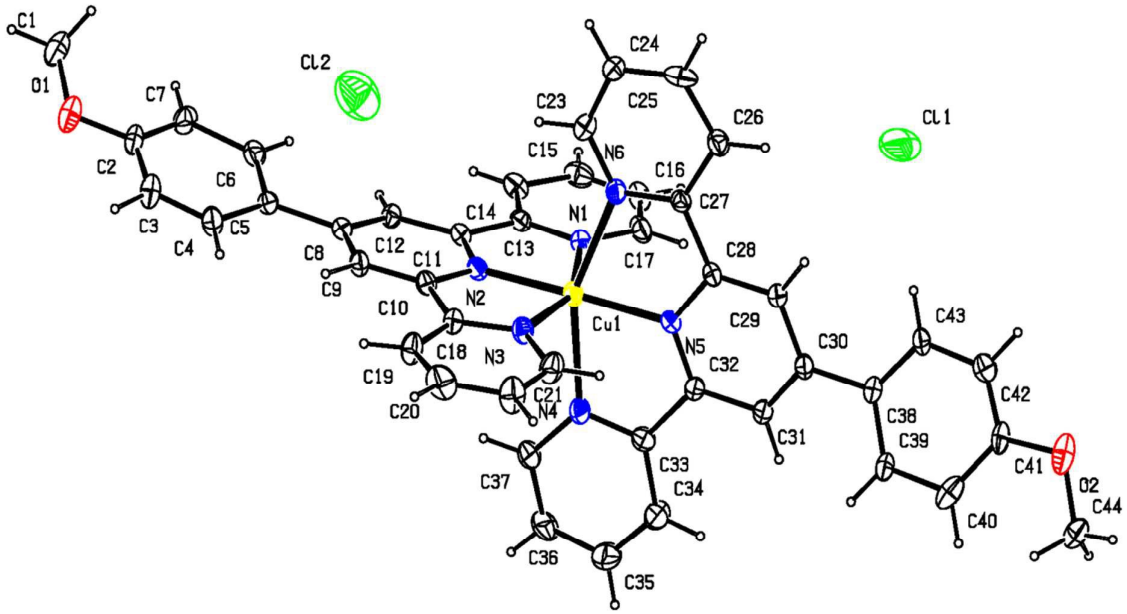

Fig. 1 ORTEP diagram of bis(terpyridine)copper(II) complex **2**·CH_3OH·$(H_2O)_6$ drawn with 50% thermal ellipsoids. The lattice methanol and water molecules are omitted for clarity.

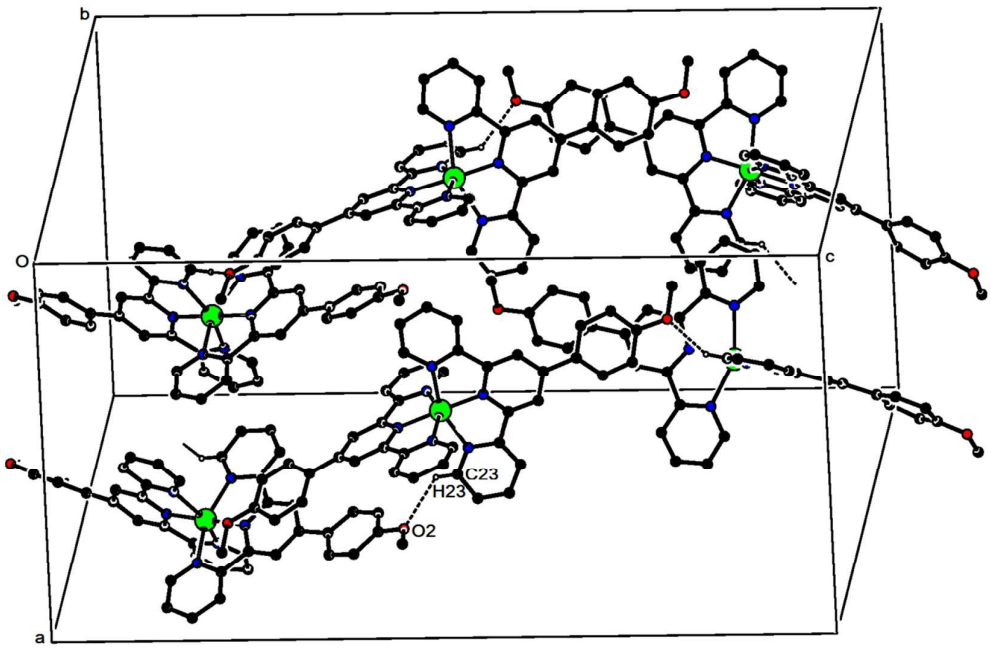

Fig. 2 The molecular packing diagram of complex **2**·CH_3OH·$(H_2O)_6$ constituted by inter molecular and intramolecular hydrogen bonds.

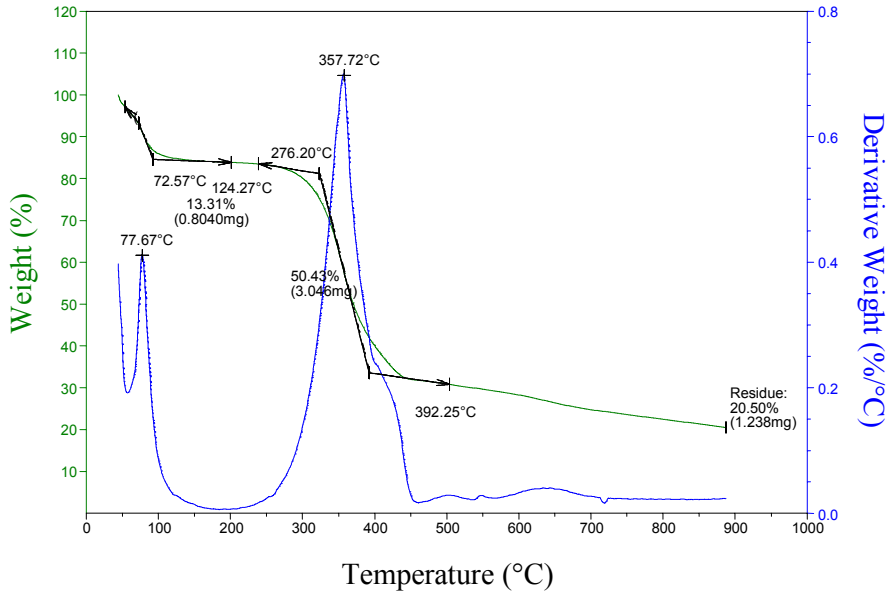

Fig. 3 TG and DTG curves of complex **2**·CH_3OH·$(H_2O)_6$.

Table 1 Crystal data and structure refinement for complex **2**·CH_3OH·$(H_2O)_6$

Empirical formula	$C_{45}H_{50}Cl_2CuN_6O_9$
Formula weight	953.35
Temperature	293(2) K
Wavelength	0.71073 Å
Crystal system	Trigonal
Space group	$P3_221$
Unit cell dimensions	a = 16.0226(4) Å, α = 90° b = 16.0226(4) Å, β = 90° c = 34.0974(12) Å, γ = 120°
Volume	7580.8(5) $Å^3$
Z	6
Density (calculated)	1.253 mg/m^3
Absorption coefficient	0.593 mm^{-1}
F(000)	2982
Crystal size	0.300 × 0.200 × 0.150 mm
Theta range for data collection	1.468 to 24.998°.
Index ranges	–19<=h<=19, –19<=k<=19, –0<=l<=40
Reflections collected	49341
Independent reflections	8444 [R(int) = 0.0873]
Completeness to theta = 24.998°	94.3%
Absorption correction	Semi-empirical from equivalents
Max. and min. transmission	0.881 and 0.756
Refinement method	Full-matrix least-squares on F^2
Data/restraints/parameters	8444/123/616
Goodness-of-fit on F^2	0.926
Final R indices [I>2sigma(I)]	R1 = 0.0659, wR2 = 0.1643
R indices (all data)	R1 = 0.1221, wR2 = 0.1873
Absolute structure parameter	0.031(9)
Largest difference peak and hole	0.484 and –0.351 $e.Å^{-3}$

Optimized geometries

The structures of complexes (**1**–**5**) were optimized using density functional theory (DFT) calculations utilizing the B3LYP functional, the LANL2DZ basis set for copper and the 6-31G(d) basis set for the remaining atoms, and the resulting optimized structures are shown in **Figure S4**. The selected bond lengths and bond angles are given in **Table S3** together with the crystallographic data of **2** for comparison. In general, the predicted bond lengths and bond angles are in agreement with the values based on the X-ray crystal structure data, and the general trends observed in the experimental data are well reproduced in the calculations. The calculated results exposed that the ground state geometries of the complexes display a distorted octahedral arrangement of ligands around the metal center. The B3LYP method in combination with the LANL2DZ basis gives an excellent estimation of Cu–N bond distances, Cu–N1, Cu–N2, Cu–N3, Cu–N4, Cu–N5, and Cu–N6.

It has been noticed that many bond lengths and bond angles obtained from the optimized structures were fitted with the experimentally observed data with a slight differences. The complex **2** with differences in bond length values of Cu–N1, Cu–N2, Cu–N3, Cu–N4, Cu–N5, and Cu–N6 are found to be 0.008, 0.009, 0.006, 0.011, 0.185 and 0.111 Å, respectively longer than the experimental data, and the difference in calculated and experimental bond angles of C(5)−N(1)−Cu, C(1)−N(1)−Cu, C(6)−N(2)−Cu, C(10)−N(2)−Cu, C(11)−N(3)−Cu, C(15)−N(3)−Cu, C(27)−N(4)−Cu, C(23)−N(4)−Cu, C(28)−N(5)−Cu, C(32)−N(5)−Cu, C(37)−N(6)−Cu, C(33)−N(6)−Cu, N(5)–Cu–N(2), N(5)–Cu–N(4), N(2)–Cu–N(4), N(5)–Cu–N(6), N(2)–Cu–N(6), N(4)–Cu–N(6), N(5)–Cu–N(3) and N(2)–Cu–N(3) are 0.1, 2.0, 1.9, 1.6, 0.0, 0.6, 0.1, 1.1, 3.3, 2.4, 2.1, 2.7, 0.6, 1.1, 0.6, 1.6, 0.8, 2.2, 1.1 and 1.4 Å, respectively (**Table S3**). Normally, the calculated bond lengths are longer than the experimental data because the former are optimized in the

gas phase and the latter are in a tight crystal lattice. In addition, theoretical calculations do not consider the effects of chemical environment.

UV-Vis absorbance spectroscopy and TD-DFT absorption spectra

UV-Vis absorption spectra of complexes (**1**−**5**) were recorded in DMF medium, which gain the valid information about the structural properties of the complexes. The complexes showed an intense absorption peak at 271–287 nm due to an intra-ligand charge transfer transition (π–π*), while strong band obtained in the range 327–338 nm is due to LMCT transition. All the complexes show a broad ligand field band in the region 716–747 nm due to metal centred d–d transition. In the case of copper(II) complexes, three d–d transitions are possible for octahedral geometry: d_{xz}, $d_{yz} \rightarrow d_{x^2-y^2}$, $d_{z^2} \rightarrow d_{x^2-y^2}$, and $d_{xy} \rightarrow d_{x^2-y^2}$. However, only a single broad band is observed for all the copper(II) complexes, which indicates the total sum of all the above transitions. The broadness associated with the d–d bands is generally taken as an indication of the geometrical distortion of the complex from perfect planar symmetry. The observed transitions suggest distorted octahedral geometry around the copper(II) ion.[46]

For more qualitative description of the experimental spectra, the nature of the transitions observed in the UV-Vis spectra of complexes (**1**–**5**) have been investigated by time dependent density functional theory (TD-DFT) at the B3LYP/6-31G(d) level. These data, with the experimental measurements, are summarized in **Table S4.** The TD-DFT absorption spectra of the complexes (**1**–**5**) show high energy absorption band involving a multitude of electronic transitions in the range 200–300 nm result from intra-ligand charge transfer transitions and involves population of the HOMO→LUMO+2 (34%) HOMO–2→LUMO+2 (2%), HOMO→LUMO (15%) HOMO–2→LUMO (9%), HOMO→LUMO (15%), HOMO–2→LUMO (27%) HOMO–1→LUMO (38%) and HOMO–2→LUMO (51%) HOMO–1→LUMO (26%) HOMO–2→LUMO+1 (2%) excitations, respectively. Further, the

bands observed in the range 300–358 nm can be attributed to the LMCT or MLCT charge transfer transitions and comprises HOMO→LUMO (40%) HOMO–2→LUMO+2 (4%) HOMO–1→LUMO (2%) HOMO–1→LUMO+1 (7%) HOMO→LUMO+1 (3%), HOMO–2→LUMO (72%) HOMO–2→LUMO+1 (3%), HOMO–1→LUMO+2 (45%) HOMO→LUMO+1 (24%) HOMO→LUMO+3 (2%), HOMO→LUMO (79%) HOMO–2→LUMO (4%) and HOMO→LUMO (74%) HOMO–2→LUMO (8%) HOMO→LUMO (2%) excitations. Finally, the spectra shows one lowest energy absorption band in the range 690–748 nm and primarily consists of HOMO–2→LUMO+2 (51%) HOMO–1→LUMO (2%) HOMO–1→LUMO+2 (8%), HOMO–1→LUMO+1 (41%) HOMO→LUMO+2 (13%) HOMO→LUMO+4 (2%), HOMO–1→LUMO+1 (34%) HOMO→LUMO+1 (12%) HOMO→LUMO+2 (46%) HOMO–1→LUMO+2 (6%), HOMO–2→LUMO (62%) HOMO–1→LUMO (23%) HOMO–2→LUMO+2 (3%) HOMO→LUMO (3%) and HOMO–1→LUMO+1 (57%) HOMO→LUMO+2 (32%) HOMO–1→LUMO (2%) HOMO–1→LUMO+3 (2%) HOMO→LUMO+1 (4%) excitations for complexes **1**–**5**, respectively (**Table S4**).

For complex **1**, the HOMO and HOMO–1 contributed 70% from ligand and 20% from metal ion, respectively whereas HOMO–2 contributed 60% metal ion and 15% ligand. The LUMO+1 contributed 80% from ligand while LUMO and LUMO+2 contributed 56% from ligand and 21% from metal ion. Thus, HOMO→LUMO is considered as major transition which is M→L transition (**Fig. 4**). Similar observations were also obtained for the complexes **2** and **3**, the HOMO and HOMO–1 contributed 46% from ligand and 17% from metal ion, respectively whereas HOMO–2 contributed 38% metal ion and 16% ligand. In the case of LUMO, LUMO+1 and LUMO+2 that contributed 19% from metal ion and 76% from ligand. Thus, HOMO→LUMO is considered as major transition, which is M→L transition (**Fig. S5** & **S6**). In the case of complex **4**, HOMO and HOMO–1 contributed 36% and

HOMO–2 contributed 13%, and LUMO, LUMO+1 and LUMO+2 contributed 11% from ligand at the same time HOMO–1, HOMO–2 and LUMO contributed 13% and LUMO+1 and LUMO+2 contributed 1% from metal ion. For the complex **5**, HOMO, HOMO–1, HOMO–2, LUMO, LUMO+1 and LUMO+2 contributes 32% from ligand and HOMO, LUMO+1 and LUMO+2 contributed 14% from metal ion (**Fig. S7**). The calculated energies and intensities are in reasonable agreement with experimental values.

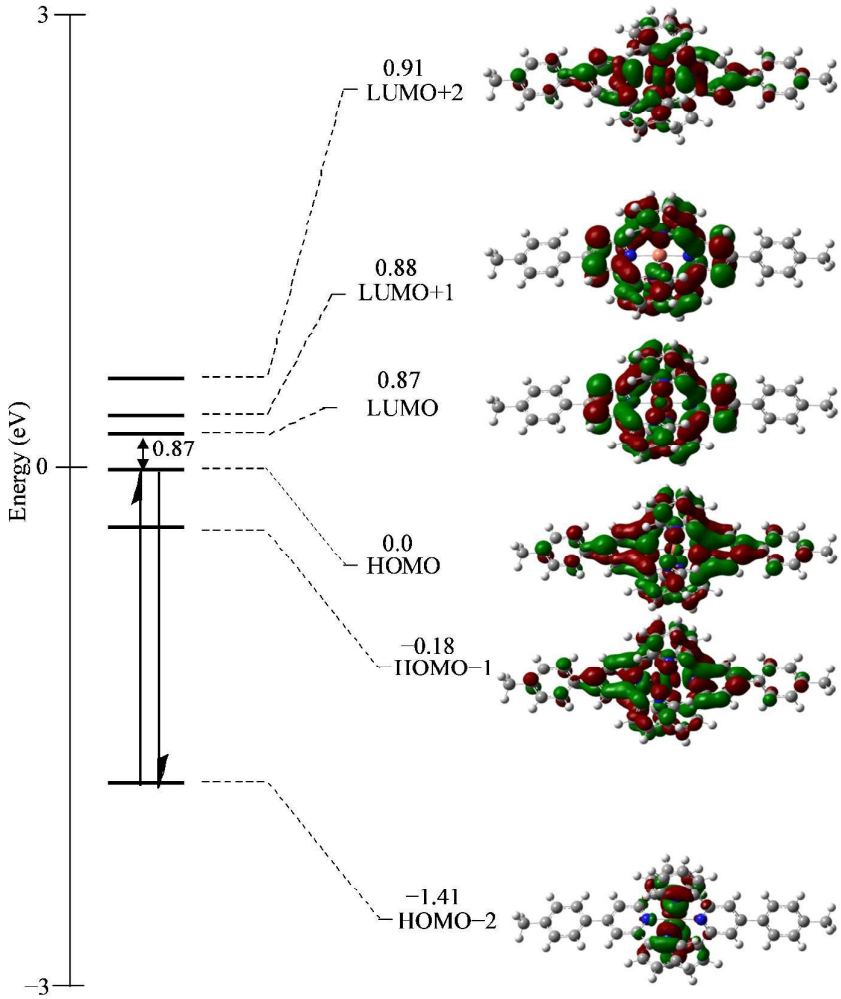

Fig. 4 Frontier MOs of complex **1**.

Frontier molecular orbitals (FMOs)

Frontier molecular orbitals play a key role in the study of electrical, optical and chemical properties.[47] Further, HOMO–LUMO energy gap reflects the chemical reactivity

and kinetic stability of the molecule. The outermost orbital containing electrons (HOMO) is the one that could act as an electron donor while the innermost (lowest energy) empty orbital (LUMO) could act as an electron acceptor. The energy gap between HOMO and LUMO is a critical parameter in determining molecular electrical transport properties.[48] A lot of applications are available for the use of HOMO–LUMO energy gap as a quantum descriptor in establishing correlation in various chemical and biochemical systems.[49] Recently, the energy gap between HOMO and LUMO has been used to prove the bioactivity from intramolecular charge transfer.[50] It is also reported that the frontier molecular orbitals are used to investigate the trend in DNA-binding of complexes and their spectral properties.[51] A molecule with a low frontier orbital gap will exhibit a significant degree of intramolecular charge transfer (ICT) from the electron-donor groups to the electron-accepter groups through π-conjugated path.[52] Moreover, complexes having high E_{HOMO} are good electron donor while those having low E_{LUMO} energy are good electron acceptor. The orbital energy level analysis for complexes **1**–**3** showed that E_{HOMO} values are –1.56, –1.75 and –2.10 eV while E_{LUMO} values are –0.63, –0.83 and –1.51 eV, respectively. The ΔE values of complexes **1**–**3** are 0.93, 0.92 and 0.59 eV, respectively. It could be noted that **3** has higher ability toward the intramolecular charge transfer than **1** and **2**. Generally, molecule having small energy gap is more polarized and is known as soft molecule. Soft molecules are more reactive than hard ones because they easily offer electrons to an acceptor. The observed small energy gap indicates that charge transfer easily occurs in it, which influences the biological activity of the molecule and low value of energy gap is also due to the groups that enter into conjugation. The calculated HOMO–LUMO energy gap agree reasonably with experimentally obtained HOMO–LUMO energy gap through liquid and solid absorption spectra.

EPR investigation

The effective magnetic moment values (1.76–1.88 BM) of complexes (**1**–**5**) are slightly higher than the spin only value (1.73 BM), which is due to the monomeric nature of complexes and there is no possibility of an exchange interaction. These values are typical for mononuclear copper(II) compounds having d^9 electronic configuration. The X-band EPR spectra show isotropic character and does not contain any hyperfine lines (**Fig. S8**), and the observed EPR spectra of the complexes are axial with $g_{\|} > g_{\perp}$, which indicates that the unpaired electron predominantly lies in the $d_{x^2-y^2}$ orbital.[53] The $g_{\|}$ and $g_{\perp}$ values of six coordinated complexes are closer to 2 ($g_{\|} > g_{\perp}$), which suggests major distortion from octahedral symmetry in the copper(II) complexes.[54] These results are further supported by the crystal structure of complex **2**. The geometric parameter, $G = (g_{\|} - 2)/(g_{\perp} - 2)$ for axial spectra measures the exchange interaction between copper(II) centers in the polycrystalline state. If $G > 4.0$, the exchange interaction is negligible and for $G < 4.0$, indicates considerable exchange interaction in the solid complexes. In the percent cases, the observed G values (1.9–2.3) of the complexes suggest the presence of exchange interaction in the copper(II) complexes.

Electrochemistry

The electrochemical properties of the complexes (**1**–**5**) were studied by cyclic voltammetry in DMF solution containing TBAP as supporting electrolyte in the potential range from 0 to –1.0 V. The cyclic voltammograms are shown in the **Fig. 5** and the data are presented in **Table S5.** The electrochemical properties of the complexes depend on the chelate ring size, axial ligation and substitution pattern in the chelate ring.[55,56] In the present case, all the complexes exhibit irreversible one electron transfer process in the range between −0.62 and −0.74 V, which can be attributed to the reduction of the metal centre. The reduction

potential of complexes **4** and **5** is less negative relative to other complexes, which indicates that the +1 oxidation state is more stabilized in complexes **4** and **5** than the other complexes.

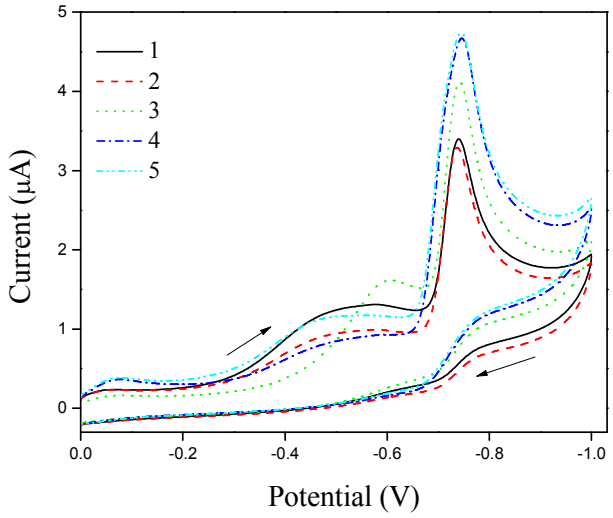

Fig. 5 Cyclic voltammograms of copper(II) complexes (**1**–**5**) in the cathodic region.

Stability of the complexes

The stability of synthesized complexes in aqueous solution were measured over different time intervals during 24, 48 and 72 h using a scanning kinetic program in UV-Vis spectrophotometer (**Fig. S9**). The UV–Vis spectra recorded directly after dilution of the complexes **1**–**3** did not show any differences after 24 and 48 h, while the 72 h samples show negligible differences, which indicate the stability of the complexes in aqueous solution.

DNA binding studies

DNA binding is the critical property for the study of effective metal based chemotherapeutic drugs, especially antitumor drugs. Therefore, the interaction between DNA and metal complexes is of importance in understanding the mechanism of binding. We have investigated the DNA binding strengths of the homoleptic bis(terpyridine)copper(II) complexes using absorption, emission, circular dichroism, hydrodynamic and electrochemical techniques.

Electronic spectral studies

In general, hyperchromism and hypochromism are the two spectral features of DNA concerning of its double helix structure; hyperchromism results from the change of the secondary structure of DNA, while hypochromism results from the contraction of DNA in the helix axis as well as from the conformational change of DNA.[57] Upon intercalation, the π* orbital of the intercalated ligand can couple with the π orbital of the DNA base pairs, decreasing the π→π* transition energy and resulting in the bathochromism. On the other hand, the coupling π orbital is partially filled by electrons, so decreasing the transition probabilities and concomitantly resulting in hypochromism.[58] The electronic absorption spectra of complexes (**1**–**5**) in the absence and presence of CT–DNA are shown in **Fig. 6**. A strong hypochromic effect in the intra-ligand transition was observed for all the complexes (25 μM) upon addition of incremental amount of DNA (0–5 μM) with a significant red-shift (4.5–6 nm). This suggests that the complexes interact with CT–DNA through the intercalative mode involving a strong interaction between complexes and the base pairs of DNA[59]. The planarity and extended aromaticity of the terpyridine ligand systems bring about the stacking of the molecule between the DNA bases. The observed trend in hypochromism among the present complexes follows the order **3** > **2** > **1** > **4** > **5**, with the binding constant (K_b) values found in the range between 1.01 (±0.06) and 3.09 (±0.12) × 10^5 M^{-1} (**Table 4**). From the binding constant values, it is clear that the complexes are moderate binders and complex **3** shows the highest binding affinity amongst them, because it has large hydrophobic contacts and π–π stacking of the DNA bases. Interestingly, the obtained binding constant values are much higher than that for other terpyridine-based copper(II) complexes[26, 60, 61] and effective anticancer drug cisplatin (3.20 ± 0.15 × 10^4 M^{-1})[62] but lower than the classical intercalator ethidium bromide in which the binding constants are in the order of 10^6–10^7 M^{-1}.[63]

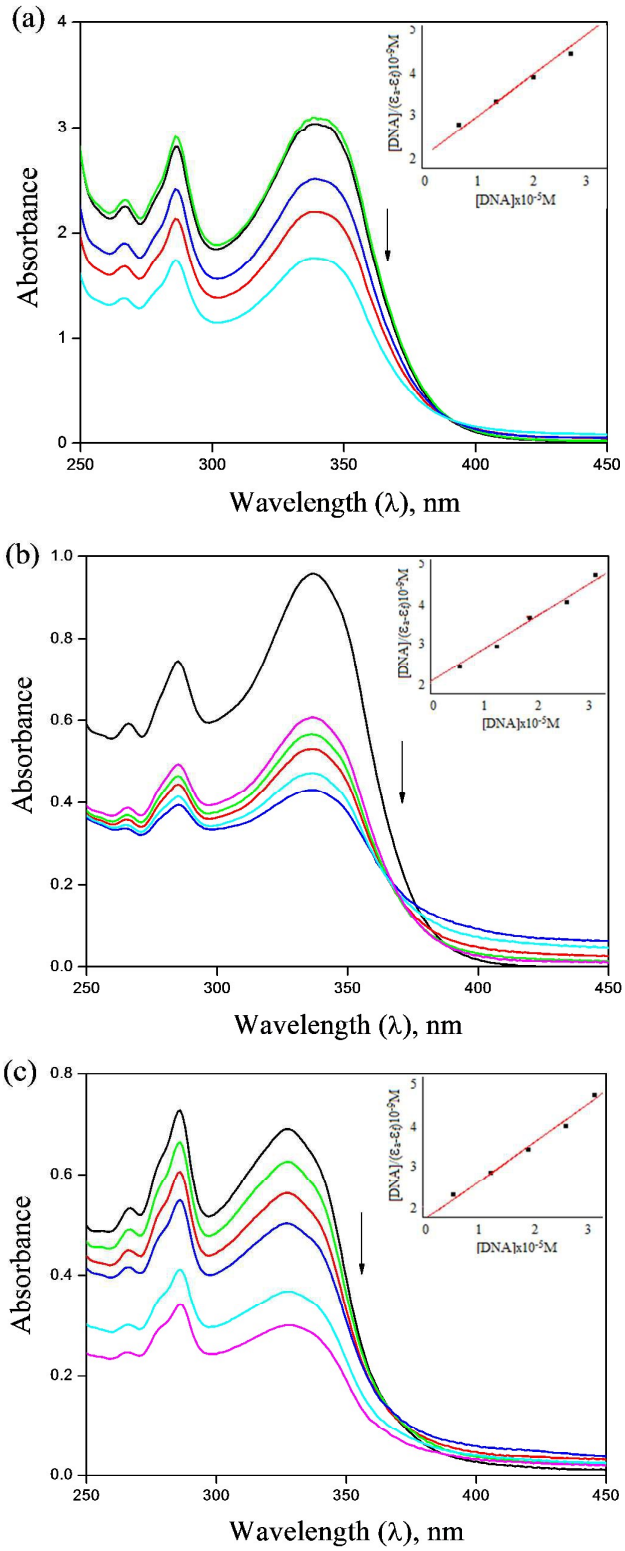

Fig. 6 Absorption spectra of complexes **1** (a), **2** (b) and **3** (c) (25 μM) in Tris-HCl buffer upon addition of CT–DNA (0–5 μM). Arrows indicate the change in absorbance upon increasing the DNA concentration. Inset: plots of [DNA]/(ε_a–ε_f) *versus* [DNA] for the titration of DNA with complexes.

Table 4 DNA-binding constants (K_b), thermal denaturation T_m (°C) and IC_{50} values of complexes against three cancerous (MCF-7, Hep-2 & HeLa) and one nontumorigenic (NHDF) cell lines

Complexes	$K_b \times 10^5$ (M^{-1})	T_m (°C)	IC_{50} values (μg/mL)*			
			MCF-7	Hep-2	HeLa	NHDF
1	1.53 ± 0.15	68.1 ± 1	17.43	23.14	21.27	93.28
2	1.62 ± 0.08	68.8 ± 1	14.82	17.18	15.14	>100
3	3.09 ± 0.12	69.4 ± 1.5	10.71	13.76	11.65	>100
4	1.09 ± 0.08	67.6 ± 0.9	–	–	–	–
5	1.01 ± 0.06	67.3 ± 0.5	–	–	–	–
Cisplatin	0.32 ± 0.02	–	16.93	17.46	17.26	>100

*Average of three independent determinations

Thermal denaturation studies

In thermal denaturation experiment, a duplex DNA is thermally denatured into single strands through the breaking of hydrogen bonding between the bases. Thermal behaviours of DNA in the presence of complex can give insight into their conformational changes when temperature is raised, and offer information about the interaction strength of complexes with DNA[64]. These experiments are also useful to provide the extent of intercalation.[65] A high ΔT_m value is suggestive of an intercalative mode of binding of the metal complex to DNA, while a low value (1–3 °C) indicates a groove and/or electrostatic binding mode.[63] The thermal denaturation experiment carried out at the wavelength of 260 nm for DNA in the absence of complex gave a T_m value of 61.0 °C (**Fig. 7**). Upon addition of complexes (**1**–**5**), T_m values increased in the range between 67.3 ± 0.5 and 69.4 ± 1.5 °C (**Table 4**). The increased ΔT_m (6.3–8.4 °C) values of the DNA after addition of the complexes is comparable to that

observed for classical intercalator,[66] suggesting the large DNA-binding affinity of the complexes.

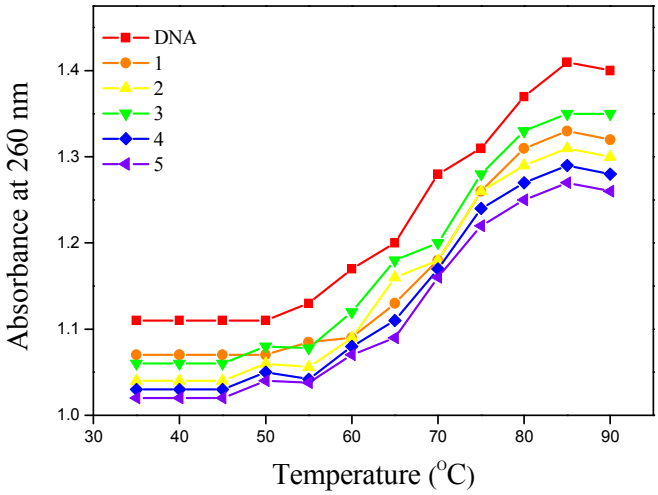

Fig. 7 Melting curves of CT–DNA (100 μM) upon addition of complexes (**1**–**5**).

Ethidium bromide displacement studies

Fluorescence spectral titrations were carried out to further investigate the binding mode of complexes with CT–DNA. Generally, DNA or EB in Tris-HCl buffer exhibit very low fluorescence intensity. However, EB is the most sensitive fluorescence probes, emits intense fluorescence at about 600 nm in the presence of DNA due to its strong intercalation between the adjacent DNA base pairs.[67] Addition of a second molecule, which may bind to DNA more strongly than EB results in a decrease of the DNA-induced EB emission. Two mechanisms have been proposed to account for this reduction in the emission intensity: the replacement of EB, and/or electron transfer.[68] If the metal complex intercalates into DNA, it leads to a decrease in the binding sites of DNA available for EB, resulting in decrease in the fluorescence intensity of the CT–DNA-EB system. The extent of decrease in the fluorescence intensity (quenching) of CT–DNA-EB reflects the extent of interaction of the complex with CT–DNA.[69] In the present study, the addition of complexes **2** and **3** (0–100 μM) to CT–DNA (10 μM) pretreated with ethidium bromide (EB 12 μM) ([DNA]/[EB] = 10) in 5 mM Tris-HCl/50 mM NaCl buffer (pH = 7.3) caused an obvious reduction in emission intensity, which

indicate the binding of complexes with DNA at the sites occupied by EB (**Fig. 8**). The observed changes clearly indicates intercalation mode of binding with CT–DNA. The quenching of EB bound to DNA by the complexes is in good agreement with the linear Stern-Volmer equation[70] $F^o/F = 1 + K_q$ [Q], where F^o and F are the fluorescence intensities in the absence and presence of complexes, respectively, K_q is a linear Stern-Volmer quenching constant, and [Q] is the concentration of complex. The slope of the plot of F^o/F *versus* [Q] gave K_q (**Fig. S10**). From a plot of the observed intensities against complex concentration the values of the apparent DNA binding constants (K_{app}) was calculated using the following equation:[71]

$$K_{EB}\,[EB] = K_{app}\,[Complex]$$

where K_{EB} is $4.94 \times 10^5\ M^{-1}$, [Complex] is the concentration of the complex used to obtain a 50% reduction in fluorescence intensity of EB.[72] The observed K_{app} values of the complexes **2** and **3** are 1.8 ± 0.11 and $2.8 \pm 0.14 \times 10^5\ M^{-1}$, respectively, which is consistent with the results obtained from absorption spectral studies. The obtained results indicates that both the complexes **2** and **3** at higher concentrations would compete with DNA-bound EB more efficiently through intercalative interaction of the terpyridine ring as well as hydrophobic interaction of substituent of terpyridine ring with the hydrophobic DNA surface.

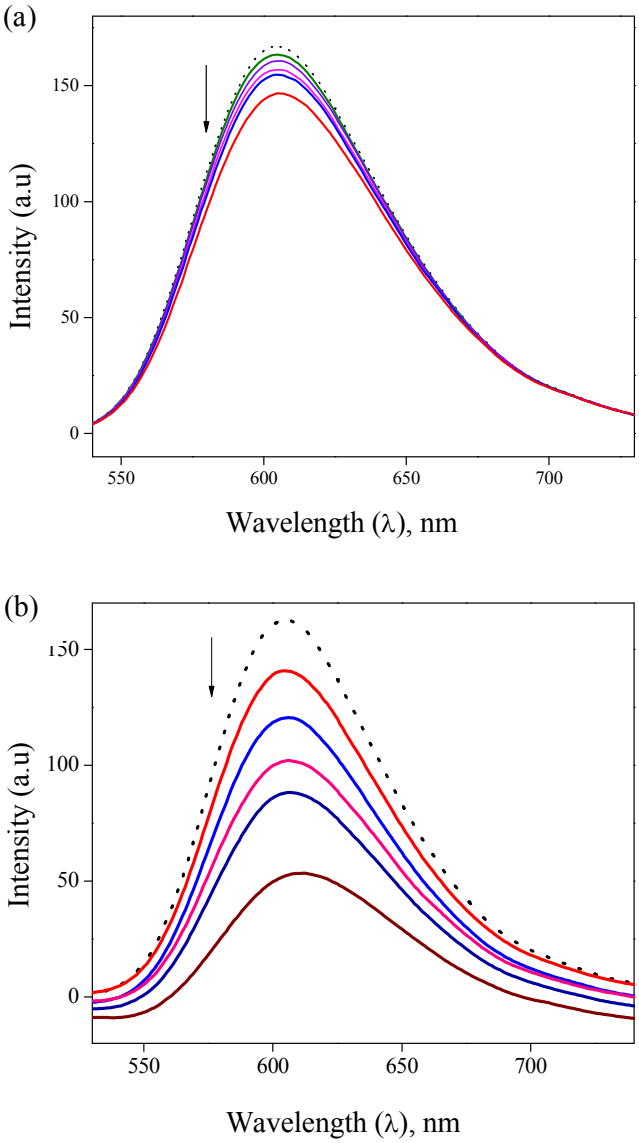

Fig. 8 Emission spectra of complexes **2** (a) and **3** (b) (0–100 μM) in Tris-HCl/NaCl buffer (pH 7.3) in the absence and presence of CT–DNA (10 μM). Arrow shows the fluorescence changes upon increasing DNA concentration.

Circular dichroic spectral studies

Circular dichroic spectra provide information about the chirality of spectroscopically active species in solution and this is a useful technique in diagnosing changes in DNA morphology during drug-DNA interactions.[73] Generally, the circular dichroism (CD) spectra of CT–DNA shows a positive band at 275 nm arising due to base stacking and a negative band at 245 nm that may be due to helicity, which is characteristic of DNA in right-handed B form.[74] Simple groove binding and electrostatic interaction of small molecules show less or

no perturbation on the base-stacking and helicity bands, whereas intercalation enhances the intensities of both the bands stabilizing the right-handed B conformation of CT–DNA as observed for classical intercalators.[75] The CD spectrum of DNA taken after incubation of the complex **3** with CT–DNA shows an increase in intensity of both negative and positive bands with a shift of 5 nm in the positive band and a small shift of 2 nm in the negative band (**Fig. 9**). Usually, the intercalative mode of binding enhances the positive Cotton effect, as has been observed in this case. These results clearly indicate intercalative binding of the complex **3** in which the complex stack in between the base pairs of DNA leading to an enhancement in the positive band.

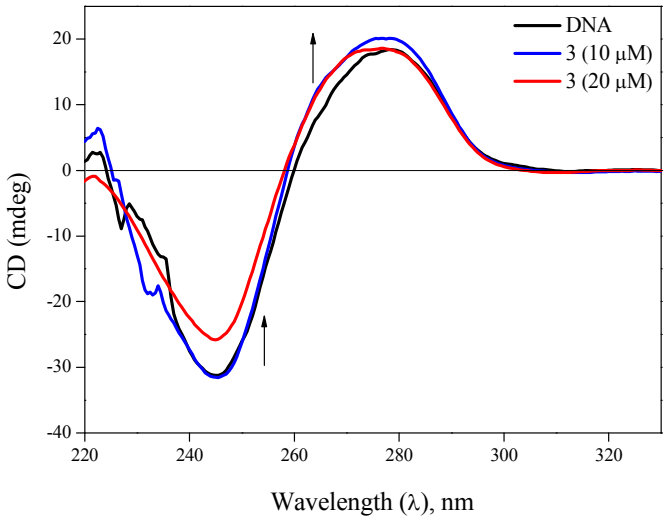

Fig. 9 CD spectrum of CT–DNA with the addition of complex **3**. Arrow shows the direction of ellipticity changes.

Hydrodynamic (viscosity) studies

To further authenticate the intercalative binding, viscosity experiments were performed, which is sensitive to changes in the length of DNA, regarded as the least ambiguous and most critical means of evaluating the binding mode of complexes with DNA in solution and can provide strong evidence for intercalative binding mode. In general, a classical intercalation model lengthens the DNA helix as the base pairs of DNA are separated on binding leading to increased DNA viscosity. In contrast, partial or non-intercalative

binding modes such as electrostatic *via* sugar-phosphate backbone may produce bend in the DNA helix reducing its effective length and viscosity, while DNA groove binding under the identical experimental conditions essentially results in less or no effect on DNA viscosity.[65] The well-known DNA intercalator EB increases the viscosity of DNA with increments of the concentration. The plots of relative viscosity $(\eta/\eta_0)^{1/3}$ *versus* binding ratio [Complex]/[DNA] are shown in **Fig S11**, which gives a measure of the viscosity changes. In the present case, relative viscosity of the DNA solutions increases greatly with increasing concentration of complexes (**1**–**5**), which is similar to that of the proven intercalator EB.[76] These observations suggest the intercalative binding of these complexes to the DNA double helix. The binding ability of complexes to increase the viscosity of DNA follows the order **3** > **2** > **1** > **4** > **5**, which is in accordance with UV-Vis absorption spectral results.

Cyclic voltammetry studies

Cyclic voltammetry is also a useful technique for investigating the interaction of the metal complexes with DNA.[77] In general, the electrochemical potential of a small molecule will shift positively when it intercalates into DNA double helix, and shift to a negative direction in the case of electrostatic interaction with DNA. In the present study, all the complexes exhibit same electrochemical behaviour upon addition of DNA, and for increasing amounts of DNA, the considerable decrease in voltammetric current (i_{pc} = 1.85–3.43) and positive shift (E_{pc} = –0.85 to –0.74) was observed, which suggest the interaction of complexes with DNA (**Fig. S12**). The decreasing extent of the peak current observed for the complexes upon addition of DNA indicates the intercalative binding mode of complexes with DNA. The decrease in peak current is much higher for complex **3** than for other complexes, which suggest its stronger binding affinity and the binding affinity follows the order **3** > **2** > **1** > **4** > **5**. The electrochemical studies corroborated well with the spectral and

viscosity studies, and thereby authenticate the strong interaction of CT−DNA with complexes **1**−**5**.

Substituent effects on DNA binding

In order to understand the influence of ligand substituents on the binding constant values, computational studies were carried out for complexes **1**–**3**, which differ only in their substituents (**Fig. S13**). Therefore, calculations were carried out by considering only the tolyl, anisole and 3,4-dimethoxybenzene substituents (**R1**, **R2** and **R3**, respectively) as representative of complexes **1**–**3**. Density functional theory (DFT) based descriptors such as chemical potential (μ), chemical hardness (η), electrophilicity (ω) and nucleus independent chemical shift (NICS) are calculated at the centre of the rings[78−80] (see section 1 of ESI for details). These four parameters are measures of reactivity and stability (**Table 5**). From the frontier molecular orbital energy gap, we can find whether the molecule is hard or soft. The chemical hardness and softness is good indicator for the chemical stability of a molecule. Generally, hardness means large energy gap whereas softness means small energy gap. In contrast, soft molecules are more polarizable than the hard ones because they need small energy for excitation. From the table, it is observed that **R3** is less hard and more reactive than **R1** and **R2**. And also, **R3** possess higher electrophilicity compared to **R2** and **R1**, indicating more reactivity of **R3** than the other two substituents. On the other hand, molecules with negative NICS values are aromatic, since negative values arise when diatropic ring current (shielding) dominates, whereas systems with positive values are antiaromatic because positive values arise when paratropic current (deshielding) dominates. NICS values indicate the degree of aromaticity: the more negative the NICS value, the more aromatic the system and higher the stability. The NICS value of **R1** and **R2** is greater than that of **R3**, indicating the higher reactivity and lesser stability of **R3**. Thus, the 3,4-dimethoxybenzene-substituted molecule (complex **3**) binds to DNA more strongly ($3.09 \pm 0.12 \times 10^5$ M^{-1}) relative to the

tolyl (complex **1**, 1.53 ± 0.15 × 10^5 M^{-1}) and anisole (complex **2**, 1.62 ± 0.08 × 10^5 M^{-1}) substituted molecules.

Table 5 Chemical potential (μ), chemical hardness (η), electrophilicity (ω) and nucleus independent chemical shift (NICS(0)) values calculated by using the B3LYP/6-31G* level of theory

Substituents	μ (eV)	η (eV)	ω (eV)	NICS(0) (ppm)
R1 (Toluene)	–3.13	3.27	1.49	–9.6
R2 (Anisole)	–3.33	3.17	1.75	–7.2
R3 (3,4-dimethoxybenzene)	–3.35	3.10	1.81	–5.8

Molecular docking with DNA

Molecular docking technique is an attractive scaffold in understanding the drug-DNA interactions to predict the exact binding site available at the molecular target DNA mainly in a non-covalent fashion, which plays an important role both for molecular recognition of nucleic acid as well as for the rational design of new chemotherapeutic drugs.[81] In our experiment, molecular docking studies of complexes (**1–5**) with DNA duplex of sequence d(CGCGAATTCGCG)$_2$ dodecamer (PDB ID:1BNA) were performed in order to predict the chosen binding site along with preferred orientation of the molecules inside the DNA groove. The docking results of complexes with DNA indicate that van der Waals interactions are dominant over electrostatic interactions (**Table S6**). Since the conformation of complexes had not changed in the minimum energy docked poses, the total internal energy reserved zero. The lower the relative binding energy, more potent is the binding affinity between the DNA and target molecules. Thus, the negative binding energy values of docked complexes suggest that they reasonably bind to DNA, and the lower binding energy value of complex **5** may be due to the lower electrostatic energy. The π-π stacking interaction between complexes and base pairs, in which the distances from the centroid of intercalative ligand to the planes of two neighboring base pairs are 3.5 and 3.6 Å, indicates that the complexes binds with

intercalation through the major groove region (**Fig. 10**). Furthermore, the energy minimized structures suggest that the complexes interact with DNA *via* an intercalation mode involving outside edge stacking interaction with oxygen atom of the phosphate backbone and A–T rich region stabilized by van der Waals interaction and hydrophobic contacts.[82,83] Thus, we can conclude that there is a mutual complement between experimental techniques and molecular docked model, which can substantiate our experimental results a nd at the same time provides further evidence of intercalation mode of bin ding.

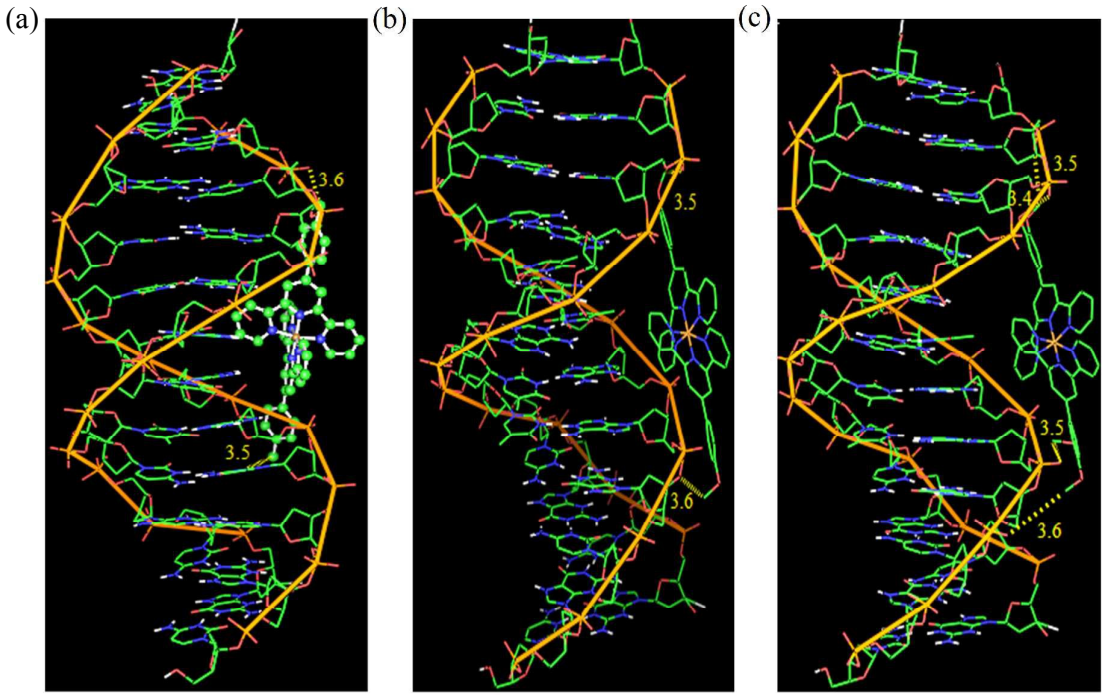

Fig. 10 Molecular docked models of complexes **1** (a), **2** (b) and **3** (c) with DNA (PDB ID: 1BNA) dodecamer duplex of sequence d(CGCGAATTCGCG)$_2$.

Protein binding studies (BSA)

The interaction between BSA and complexes is of important to understand their uptake, bio-distribution, overall toxicity, mechanism of action and shuttling of the complexes to cancer cells, and hence we have explored the interaction of these complexes with BSA using absorption and emission spectroscopy.

UV-Vis absorption studies of BSA

UV-Vis absorption spectra is the tool to determine the type of quenching involved in the binding process. The fluorescence quenching mechanisms are either dynamic or static quenching. In dynamic quenching mechanism, the absorption spectra of the fluorescent substance is not changed, and only the excited state fluorescence molecule is influenced by quenchers, while for static quenching, a new compound is formed between the ground state of the fluorescent substance and quencher, which considerably influences the absorption spectra of fluorescence substance.[84] The electronic absorption spectra of complexes (**1**−**5**) in the absence and presence of BSA are shown in **Fig. 11**. It can be clearly seen from the figure that the absorption intensity of BSA at 280 nm increases after incubation with the copper(II) complexes with small red shift of ~3 nm. This observation suggested a static interaction between BSA and the complexes.[85, 86]

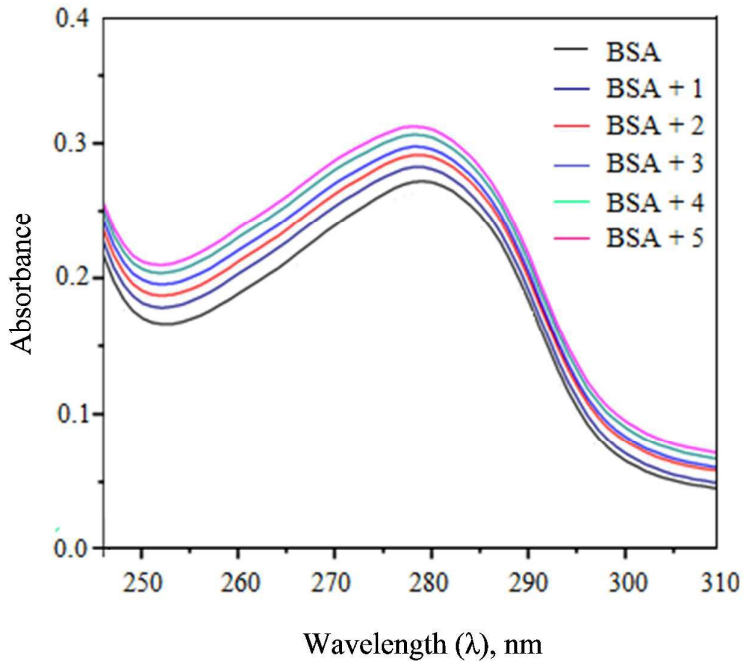

Fig. 11 Absorbance titrations of the complexes **1**−**5** with BSA.

Fluorescence spectrometry of BSA

Fluorescence spectroscopy has proved to be an efficient tool in detecting the quenching mechanism, mode and strength of the interaction of BSA with drugs.[87] The

presence of the amino acids tryptophan, tyrosine and phenylalanine results in the intrinsic fluorescence of BSA,[88] and quenching is usually induced by a variety of molecular interactions such as excited-state reactions, molecular rearrangements, energy transfer, ground-state complex formation and collision quenching.[89] If the tyrosine is ionized, then its fluorescence is completely quenched, whereas phenylalanine has a very low quantum yield. This means that intrinsic fluorescence of BSA is due to tryptophan alone. Therefore, fluorescence behavior of BSA can provide significant information about the structure, dynamics, and protein folding. A solution of BSA (10 μM) was titrated with various concentrations of the complex **3** (0−50 μM) in the range of 280−420 nm (λ_{ex} 280 nm), which resulted in the quenching of fluorescence quenching intensity (**Fig. 12**). The observed results indicates the changes in the protein secondary structure as well as the tryptophan environment of BSA upon binding with the complexes.[90] The fluorescence intensity of BSA at ~348 nm was quenched with red shifts by the complex **3** (75%, 2 nm). The obtained red shift primarily arises due to the presence of the active site of the protein in a hydrophobic environment and suggest the interaction between the complex and BSA.[91] The quenching constant (Kq) was evaluated following Stern-Volmer and Scatchard equation:[92]

$$\text{Log } [I_0–I/I] = \log K_{bin} + n \log [Q]$$

where K_{bin} is the binding constant of the complex with BSA and n is the number of binding sites. The number of binding sites (n) and the binding constant (K_{bin}) have been found from the plot of log $(I_0–I)/I$ *versus* log [Q] (**Fig. S14**).

The values of K_{bin}, Kq and n obtained for the binding of BSA to the copper(II) complex **3** is given in **Table S7**. The larger values of K_{bin} and Kq indicate a strong interaction between the BSA protein and the complex. The higher protein-binding affinity of complex **3** is due to the enhanced hydrophobicity provided by the substituent of the 4'-(3,4-dimethoxyphenyl)-2,2':6',2''-terpyridine ligand.

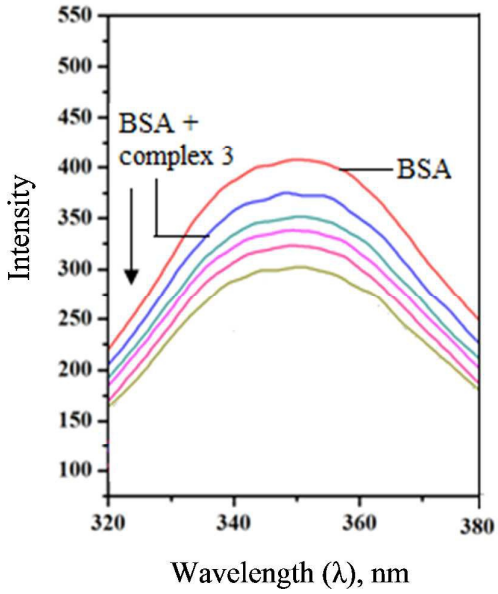

Fig. 12 Emission spectra of BSA (10 μM; λ_{ex} = 280 nm; λ_{em} = 348 nm) in the presence of increasing amounts of **3** (10-50 μM). Arrow shows that emission intensity changes upon increasing the concentration of complex.

Molecular docking with *c*-Met kinase

A primary hurdle in developing anticancer therapeutics is selective target of cancer cells while sparing normal tissues. *c*-Met is a receptor tyrosine kinase (RTK) that has low activity in normal tissues but is dysregulated in many tumor types. It is the only known high affinity receptor for hepatocyte growth factor (HGF), also known as scatter factor.[93] *c*-Met and HGF are both required for normal mammalian development.[94] Further, the results of *in vitro* and *in vivo* experiments show that this receptor-growth factor pair is involved in multiple physiological cellular responses including embryogenesis, cell proliferation, survival, differentiation, motility, migration, angiogenesis, metastasis, invasion and drug resistance.[95–97] Therefore, for the above said reasons, we have selected the *c*-Met tyrosine kinases receptor for docking studies. This study on the interaction of copper complexes with BSA helps to understand how the drug molecules may affect the structure of proteins when drugs are introduced to target specific diseases. Descriptions of the 3D structure of crystalline albumin have revealed that BSA comprises three homologous domains (I, II, and III), each

domain contains two subdomains (A and B), and they are divided into nine loops by 17 disulfide bonds, each one formed by six helices, and its secondary structure is dominated by α-helix.[98] BSA can bind with drugs in several binding sites and the principal regions of drug binding to BSA are located in the hydrophobic cavities in subdomains IIA and IIIA.[99] The predicted active sites consisted of amino acids such as Val1083, Ile1084, Gly1085, Arg1086, Val1092, Ala1108, Leu1140, Tyr1159, Met1160, Lys1161, His1162, Gly1163, Asp1164, Asn1167, Phe1168, Asn1171, Thr1173, Arg1208, Asn1209, Met1211, Ala1221, Ash1222, Tyr1230 and Asp1231.

The glide approximates a complete systematic search of the conformational, orientational, and positional space of the docked complexes. Selection of the best docked pose is done based on empirical and force-field-based terms. Molecular docking was employed using glide to understand the non-bonding interaction between the copper complexes **1**–**3** and BSA (**Fig. S15**). The results reveal that the complexes was half-surrounded within subdomain IIA hydrophobic cavity, and it is in close proximity to hydrophobic residues such as Val1083, Ile1084, Val1092, Ala1108, Leu1140, Tyr1159, Met1160, Phe1168, Met1211, Ala1221 and Tyr1230 suggesting the existence of hydrophobic interaction between them. The complexes **1**–**3** with binding free energy of –13.195, –16.145 and –29.442 KJmol^{-1}, respectively indicating the more potent binding affinity between *c*-Met tyrosine kinase receptor and complex **3**. The docked complex **1** shown in the ball and stick form against the tyrosine kinase *c*-Met with electrostatic potential surface and interacting residues is presented in **Fig 13**. Complex **3** shows a large hydrophobic cavity in subdomain IIA, which play an important role in absorption, metabolism, and transportation of BSA, and the complex **2** and the residue Tyr1230 connected by π–π stacking interactions. The results obtained from molecular docking indicate that the interaction between complexes and BSA was dominated by hydrophobic forces as well as π–π stacking, thereby suggesting the good

binding affinity of the homoleptic copper(II) complexes with the receptor, which may be deemed as one of the reasons for the successful elimination of cancer cells in the anticancer studies.

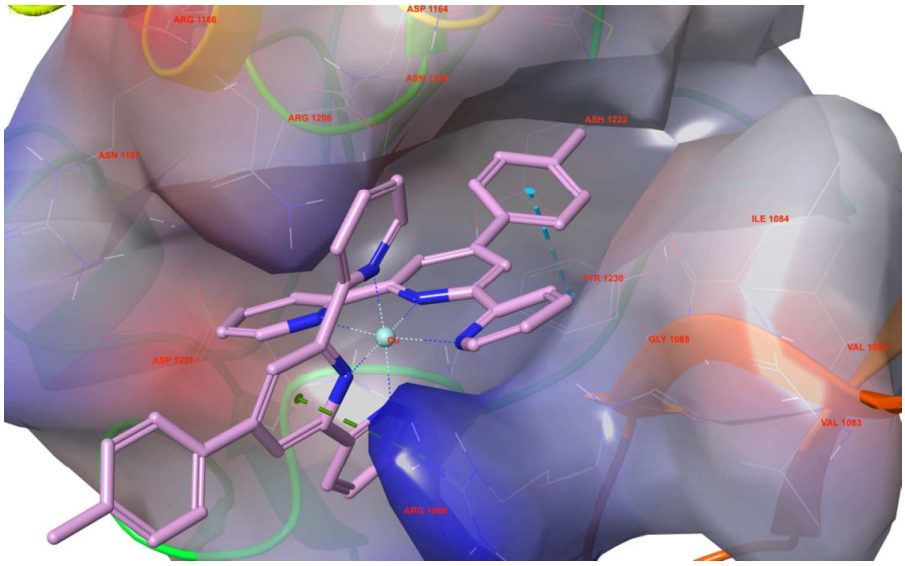

Fig. 13 Molecular docked model of complex **1** located within the hydrophobic pocket of BSA.

DNA cleavage activity

Some of the anticancer agents approved for clinical use trigger cell death by damaging DNA and the antitumor activities of several tested copper(II) complexes are in good correlation with the DNA cleavage activities.[16, 100] The interaction between metal complex and dioxygen or redox reagents are believed to be the major cause of DNA damage. The ability of the complexes (**1**–**3**) to bring about DNA cleavage was assessed from the conversion of supercoiled DNA (Form I) to nicked circular (Form II) and linearized (Form III) forms. It has been known that certain copper(II) complexes cleave DNA with H_2O_2 *via* Fenton catalyst.[101] Therefore, DNA cleavage activity of complexes **1**–**3** in the presence of H_2O_2 were tested, in which the complexes convert SC DNA into NC form revealing that these complexes behave as chemical nucleases in the presence of co-oxidant (**Fig. S16a**). In agarose gel electrophoresis, supercoiled DNA migrates faster while linear

form migrates between supercoiled and nicked circular form. In order to study the potential mechanism of DNA cleavage mediated by complexes the quenching assay of pBR322 DNA were studied in the presence of some standard radical scavengers such as hydroxyl radical scavenger (DMSO), singlet oxygen quencher (NaN_3) and superoxide oxygen scavenger (SOD) under identical conditions (**Fig. S16b**).

The experimental results show that the addition of hydroxyl radical scavenger DMSO strongly inhibits the DNA cleavage, suggesting the involvement of hydroxy radicals in the cleavage process (Lane 5–7). On the other hand, no inhibition in the DNA cleavage activity was observed in the presence of singlet oxygen quencher NaN_3 and superoxide radical scavenger SOD (Lanes 2–4 and 8–10, respectively). Therefore, the presence of singlet oxygen and superoxide ion should be ruled out of the DNA cleavage process. The result clearly shows that the hydroxyl radical produced by hydrogen peroxide is responsible for the observed DNA cleavage.

Cytotoxic studies

MTT assay

The balance between the therapeutic potential and toxic side effects of a compound is very important when evaluating its usefulness as a pharmacological drug. In these contest, the experiments were designed to investigate the *in vitro* cytotoxicity of synthesized homoleptic copper(II) complexes (**1**–**3**) and a benchmark compound cisplatin against three cancer cell lines such as human breast adenocarcinoma (MCF-7), epithelioma (Hep-2) and cervical (HeLa), and one nontumorigenic human dermal fibroblasts (NHDF) cell line by MTT assay. The MTT assay has been widely used to measure the cell proliferation rate based on the fact that live cells reduce yellow MTT to blue formazan products. Further, this assay indirectly suggests the metabolic status of the cells and the events that lead to necrosis or apoptosis. In the present cytotoxic analysis, various concentration (2, 5, 10, 25, 50 and 100 μM) of

homoleptic copper(II) complexes were tested for 48 h. The complexes were dissolved in 0.1% DMSO and a blank sample containing the same volume of DMSO was taken as a control to identify the activity of the solvent. The cell viability was concentration-dependent, which decreased with increasing concentrations of complexes, and the IC_{50} values are given in **Table 4**. Further, all the complexes exhibit potent cytotoxicity against all the cancer cells. The antiproliferative efficiency of complexes **1**–**3** on the nontumorigenic NHDF cells is much lower than that on the other three tumorigenic cell lines. Interestingly, the complex **3** showed highest anticancer activity against three cancer cell lines such as MCF-7, Hep-2 and HeLa, which was more potent than the positive control cisplatin. The high cytotoxicity of the complexes may originate from the strong hydrophobic interaction of the complexes with both DNA and protein. Interestingly, the IC_{50} values are much lower than that for previously reported bis(terpyridine) complexes.[102,103] These results suggest that they possess high selectivity between cancer and normal cells and display potential application in cancer chemoprevention and chemotherapy.

Hoechst staining studies

Apoptosis or programmed cell death is a highly conserved, tightly controlled cell suicide process that is regulated by many different intracellular and extracellular events to ablate neoplastic cells in normal physiological functions. Apoptosis is controlled by two potential pathways, the mitochondrial pathway and the death receptor pathway. The mitochondrial pathway is characterized by the loss of mitochondrial transmembrane potential and release of cytochrome *c*.[104] The death receptor pathway is mediated by serial activation of Fas [a cell surface death receptor of the tumor necrosis factor (TNF) family of cytokines]. Apoptosis as an intrinsic suicide serving to remove excess, damaged or infected cells in metazoans, and characterized by a variety of morphological and biochemical events including

phosphatidylserine (PS) externalization, chromatin condensation, genomic DNA fragmentation and plasma-membrane blebbing.[105]

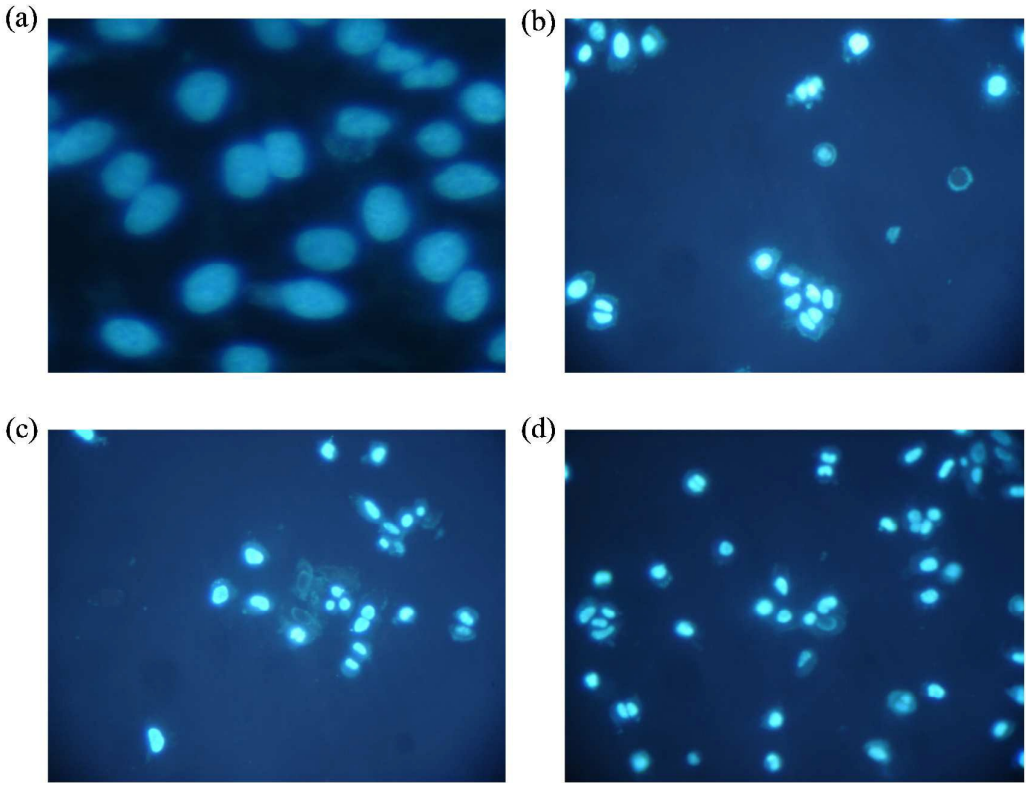

Fig. 14 Hoechst 33258 staining of MCF-7 cells for 48 h, control (a), complexes **1** (b), **2** (c) and **3** (d).

Apoptotic effect of the synthesized complexes **1**−**3** was studied on MCF-7 cells by Hoechst dye staining method. In this method, an observation was made among the sample treated cells with untreated cells. Extensive apoptotic alterations were observed in complex **3** (50 µg/mL) after 48 h and the order of apoptotic activity was as follows: **3** > **2** > **1**. The envoy morphological changes observed such as chromatin fragmentation, bi- and/or multinucleation, cytoplasmic vacuolation, nuclear swelling, cytoplasmic blebbing and late apoptosis indication of dot-like chromatin condensation (**Fig. 14**). The obtained morphological changes suggest that complex **3** possesses higher efficiency than **1** and **2** in killing the cells by apoptosis (**Table. S8**). The higher apoptosis-inducing ability of the complex **3** was consistent with the hydrophobicity of the 4'-(3,4-dimethoxyphenyl)-2,2':6',2''-

terpyridine, which facilitates the migration of the complex across the cell membrane and its eventual release at various organelles to bind with DNA leading to apoptosis, and account for their higher anti-proliferative activity.

Conclusions

A series of homoleptic bis(terpyridine)copper(II) complexes of the type $[Cu(L^{1-5})_2]Cl_2$ (**1–5**) have been synthesized and characterized. The single crystal XRD structure of the complex **2** revealed distorted octahedral geometry around copper ion. Structural parameters from the crystallographic and DFT studies are in good agreement with each other. Additionally, the DFT studies revealed the possible charge transfer taking place within the molecule and the obtained smaller energy gap supports the bioefficacy of the complexes. All the complexes exhibited intercalative mode of binding to CT−DNA, further supported by thermal denaturation and molecular docking studies. The experimental results of interaction between the complexes and BSA protein support static quenching mechanism, and this information will be useful in understanding the binding of drugs to protein. The BSA docking studies revealed hydrophobic, π-π stacking and hydrogen bonding interaction between the bis(terpyridine)copper(II) complexes and *c*-Met kinase receptor located within subdomain IIA cavity. All the complexes show significant DNA cleavage activity in the presence of hydrogen peroxide. The complexes **1**–**3** display cytotoxicity against three different cancer cell lines but are non-toxic to normal cells. All the complexes have found to be more cytotoxic against three cancer cell lines than the widely used drug cisplatin with respect to their IC_{50} values. The complex **3** is remarkable in displaying a higher cytotoxicity when compared to other complexes, which is consistent with their effective interaction with DNA as well as cellular protein. These bis(terpyridine)copper(II) complexes inhibit the growth of three different cancer cell lines, which may provide the basis for the design of potentially effective target-specific drugs for the treatment of cancer.

Supplementary material

Electronic supplementary information (ESI) available. CCDC 1406261 contains the supplementary crystallographic data for complex **2**. These data can be obtained free of charge from http://www.ccdc.cam.ac.uk/conts/retrieving.html or from the CCDC 12 Union Road, Cambbridge CB2 1EZ, UK; Fax: +44-1223-336033; e-mail: deposit@ccdc.cam.ac.uk.

Acknowledgements

We are thankful to Dr. Babu Varghese, SAIF, Indian Institute of Technology Madras (IIT-M), Chennai-600 036, for his help in solving crystal structure. We are also thankful to Dr. Devaraj Vinod, College of Pharmacy, Madras Medical College, Chennai-600 003, for his help in BSA docking studies using Schrödinger software.

References:

1. I. Haq and J. Ladbury. *J. Mol. Recognit*., 2000, **13,** 188–197.
2. M.J. Hannon. *Chem. Soc. Rev*., 2007, **36,** 280–295.
3. Z. Guo and P.J. Sadler, *Angew. Chem. Int. Ed*., 1999, **38,** 1512–1531;
4. K.H. Thompson and C. Orving, *Science,* 2003, **300,** 936–939.
5. K.D. Mjos and C. Orving, *Chem. Rev*., 2014, **114,** 4540–4563.
6. I. Bertini, H.B. Gray, S. Lippard and J. Valentine, Bioinorganic Chemistry; University Science Books: Sausalito, CA, 1994.
7. K.E. Erkkila, D.T. Odom and J.K. Barton, *Chem. Rev.,* 1999, **99,** 2777–2796.
8. L. Kelland, *Nat. Rev. Cancer,* 2007, **7,** 573–584.
9. B. Lippert, Ed., Cisplatin Chemistry and Biochemistry of a Leading Anticancer Compound, Hevetica Chimica Acta/Wiley-VCH, Zurich, Switzerland, 1999.
10. P.C.A. Bruijnincx and P.J. Sadler, *Curr. Opin. Chem. Biol.,* 2008, **12,** 197–206.
11. R. Ren, P. Yang, W. Zheng and Z. Hua, *Inorg. Chem.,* 2000, **39,** 5454–5463.
12. D. Palanimuthu, S.V. Shinde, K. Somasundaram and A.G. Samuelson, *J. Med. Chem.,* 2013, **56,** 722–734.
13. C. Santini, M. Pellei, V. Gandin, M. Porchia, F. Tisato, and C. Marzano, *Chem. Rev.,* 2014, **114,** 815–862.
14. S.C. Zhang, Y.G. Zhu, C. Tu, H.Y. Wei, Z. Yang, L.P. Lin, J. Ding, J.F. Zhang and Z.J. Guo, *J. Inorg. Biochem.,* 2004, **98,** 2099–2106.
15. P.U. Maheswari, M. van der Ster, S. Smulders, S. Barends, G.P. van Wezel, C. Massera, S. Roy, H. den Dulk, P. Gamez and J. Reedijk, *Inorg. Chem.,* 2008, **47,** 3719–3727.
16. R. Loganathan, S. Ramakrishnan, E. Suresh, A. Riyasdeen, M.A. Akbarsha and M. Palaniandavar, *Inorg. Chem.,* 2012, **51,** 5512–5532.
17. K.C. Jantunen and B.L. Scott, *J. Am. Chem. Soc.,* 2006, **128,** 6322–6323.

18. J.M. Lehn, Supramolecular Chemistry, Concepts and Perspectives; VCH: Weinheim, 1995.

19. G. Chelucci and R.P. Thummel, *Chem. Rev.,* 2002, **102,** 3129–3170.

20. P.B. Glover, P.R. Ashton, L.J. Childs, A. Rodger, M. Kercher, R.M. Williams, L.D. Cola and Z. Pikramenou, *J. Am. Chem. Soc.,* 2003, **125,** 9918–9919.

21. K. Szaciłowski, W. Macyk, A. Drzewiecka-Matuszek, M. Brindell and G. Stochel, *Chem. Rev.,* 2005, **105,** 2647–2694.

22. C.K.L. Li, R.W.Y. Sun, S.C.F. Kui, N. Zhu and C.M. Che, *Chem.–Eur. J.,* 2006, **12,** 5253–5266.

23. P.P. Silva, W. Guerra, J.N. Silveira, A.M. da C. Ferreira, T. Bortolotto, F.L. Fischer, H. Terenzi, A. Neves and E.C. Pereira-Maia, *Inorg. Chem.,* 2011, **50,** 6414–6424.

24. M. O'Connor, A. Kellett, M. McCann, G. Rosair, M. McNamara, O. Howe, B.S. Creaven, S. McClean, A.F.-A. Kia, D. O'Shea and M. Devereux, *J. Med. Chem.,* 2012, **55,** 1957–1968.

25. V. Uma, M. Kanthimathi, T. Weyhermuller and B.U. Nair, *J. Inorg. Biochem.,* 2005, **99,** 2299–2307.

26. V. Uma, M. Elango and B.U. Nair, *Eur. J. Inorg. Chem.,* 2007, 3484–3490.

27. V.M. Manikandamathavan, R.P. Parameswari, T. Weyhermüller, H.R. Vasanthi and B.U. Nair, *Eur. J. Med. Chem.,* 2011, **46,** 4537–4547.

28. R. Indumathy, M. Kanthimathi, T. Weyhermuller and B.U. Nair, *Polyhedron,* 2008, **27,** 3443–3450.

29. G. Sathyaraj, T. Weyhermuller and B.U. Nair, *Eur. J. Med. Chem.,* 2010, **45,** 284–291.

30. A. Kumar, J.P. Chinta, A.K. Ajay, M.K. Bhat and C.P. Rao, *Dalton Trans.,* 2011, **40,** 10865–10872.

31. U. Basu, I. Khan, D. Koley, S. Saha, P. Kondaiah and A.R. Chakravarty, *J. Inorg. Biochem.,* 2012, **116,** 77–87.

32. A. Juneja, T.S. Macedo, D.R.M. Moreira, M.B.P. Soares, A.C.L. Leite, J.K.de.A.L. Neves, V.R.A. Pereira, F. Avecilla and A. Azam, *Eur. J. Med. Chem.,* 2014, **75,** 203–210.

33. D. Mahendiran, P. Gurumoorthy, K. Gunasekaran, R.S. Kumar and A.K. Rahiman, *New J. Chem.,* 2015, **39,** 7895–7911.

34. J. Wang and G.S. Hanan, *Synlett.,* 2005, **8,** 1251–1254.

35. G. M. Sheldrick, SHELXL 2014/7, University of Göttingen, Germany, 2014.

36. M.J. Frisch, G.W. Trucks, H.B.H. Schlegel, G.E. Scuseria, M.A. Robb, J.R. Cheeseman, V.G. Zakrzewski, J.A. Montgomery, R.E. Stratmann, J.C. Burant, S. Dapprich, J.M. Millam, A.D. Daniels, K.N. Kudin, M.C. Strain, O. Farkas, J. Tomasi, V. Barone, M. Cossi, R. Cammi, B. Mennucci, C. Pomelli, C. Adamo, S. Clifford, J. Ochterski, G.A. Petersson, P.Y. Ayala, Q. Cui, K. Morokuma, D.K. Malick, A.D. Rabuck, K. Raghavachari, J.B. Foresman, J. Cioslowski, J.V. Ortiz, A.G. Baboul, B.B. Stefanov, G. Liu, A. Liashenko, P. Piskorz, I. Komaromi, R. Gomperts, R.L. Martin, D.J. Fox, T. Keith, M.A. Al-Laham, C.Y. Peng, A. Nanayakkara, C. Gonzalez, M. Challacombe, P.M.W. Gill, B.G. Johnson, W. Chen, M.W. Wong, J.L. Andres, M. Head-Gordon, E.S. Replogle and J.A. Pople, Gaussian 03 (Revision A.9), Gaussian, Inc., Pittsburgh, 2003.

37. A.D. Becke, *J. Chem. Phys.,* 1993, **98,** 5648–5652.

38. J. Marmur, *J. Mol. Biol.,* 1961, **3,** 208–218.

39. P. Arthi, S. Shobana, P. Srinivasan, L. Mitu and A.K. Rahiman, *Spectrochim. Acta A,* 2015, **143,** 49–58.

40. A.I. Huguet, S. Manez and M.J. Alcaraz, *Z. Naturforsch,* 1990, **45,** 19–24.

41. T. Mosmann, *J. Immuno. Methods,* 1983, **65,** 55–63.

42. R. Bergan, E. Kyle, P. Nguyen, J. Trepel and L. Neckers *Clin. Exp. Metastasis,* 1996, **14,** 389–398.

43. P. Kubelka and F. Munk, *Tech. Z. Phys.,* 1931, **12,** 593–601.

44. T.H. Rakha, K.M. Ibrahim and M.I. Khalifa, *Thermochim. Acta,* 1989, **144,** 53–63.

45. S.A. Sadeek, M.S. Refat, S.M. Teleb and S.M. El-Megharbel, *J. Mol. Struct.,* 2005, **737,** 139–145.

46. J.C. Bailar, H.J. Emeleus, S.R. Nyholm and A.F.T. Dickenson, Comprehensive Inorganic Chemistry, vol. 3, Pergamon Press, 1975.

47. I. Fleming, Frontier Orbitals and Organic Chemical Reactions, John Wiley and Sons, New York, 1976.

48. K. Fukui, *Science,* 1982, **218,** 747–754.

49. D.F.V. Lewis, C. Ioannides and D.V. Parke, *Xenobiotica,* 1994, **24,** 401–408.

50. C. Ravikumar, I.H. Joe and V.S. Jayakumar, *Chem. Phys. Lett.,* 2008, **460,** 552–558.

51. A. G. Quiroga, J. M. Perez, I. Lopez-Solera, E. I. Montero, J. R. Masaguer, C. Alonso and C. Navarro-Ranninger. *J. Inorg. Biochem.,* 1998, **69,** 275–281.

52. T.S. Xavier, N. Rashid and I.H. Joe, *Spectrochim. Acta Part A,* 2011, **78,** 319–326.

53. M. Bose, K. Ohta, Y. Babu and M. D. Sastry, *Chem. Phys. Lett.,* 2000, **324,** 330–336.

54. M. Shebl, *J. Coord. Chem.,* 2009, **62,** 3217–3231.

55. F.V. Lovecchino, E.S. Gore and D.H. Bush, *J. Am. Chem. Soc.,* 1974, **96,** 3104–3109.

56. P.A. Conmick and K.A. Macor, *Inorg. Chem.,* 1991, **30,** 4654–4663.

57. E.C. Long and J.K. Barton, *Acc. Chem. Res.,* 1990, **23,** 271–273.

58. A.M. Pyle, J.P. Rehmann, R. Meshoyrer, C.V. Kumar, N.J. Turro and J.K. Barton, *J. Am. Chem. Soc.,* 1989, **111,** 3053–3063.

59. J.K. Barton, A.T. Danishefsky and J.M. Golberg, *J. Am. Chem. Soc.,* 1984, **106,** 2172–2176.

60. V.M. Manikandamathavan, T. Weyhermüller, R.P. Parameswari, M. Sathishkumar, V. Subramanian and B.U. Nair, *Dalton Trans.,* 2014, **43,** 13018–13031.

61. S. Rajalakshmi, M.S. Kiran and B.U. Nair, *Eur. J. Med. Chem.,* 2014, **80,** 393–406.

62. F. Arjmand, F. Sayeed and D. Muddassir. *J. Photochem. Photobiol. B,* 2011, **103,** 166–179.

63. M. Cory, D.D. Mckee, J. Kagan, D.W. Henry and J.A. Miller, *J. Am. Chem. Soc.,* 1985, **107,** 2528–2536.

64. Y.J. Liu, H. Chao, L.F. Tan, Y.X. Yuan, W. Wei and L.N. Ji, *J. Inorg. Biochem.,* 2005, **99,** 530–537.

65. J.M. Kelly, A.B. Tossi, D.J. McConnell and C. OhUigin, *Nucl. Acids Res.,* 1985, **13,** 6017–6034.

66. G.A. Neyhart, N. Grover, S.R. Smith, W.A. Kalsbeck, T.A. Fairly, M. Cory and H.H. Thorp, *J. Am. Chem. Soc.,* 1993, **115,** 4423–4428.

67. F.J. Meyer-Almes and D. Porschke, *Biochemistry,* 1993, **32,** 4246–4253.

68. R.F. Pasternack, M. Cacca, B. Keogh, T.A. Stephenson, A.P. Williams and F.J. Gibbs, *J. Am. Chem. Soc.,* 1991, **113,** 6835–6840.

69. J. B. Lepecq and C. Paoletti, *J. Mol. Biol.,* 1967, **27,** 87–106.

70. K. S. Ghosh, B. K. Sahoo, D. Jana and S. Dasgupta, *J. Inorg. Biochem.,* 2008, **102,** 1711–1718.

71. M. Lee, A. L. Rhodes, M. D. Wyatt, S. Forrow and J. A. Hartley, *Biochemistry,* 1993, **32,** 4237–4245.

72. S. Satyanarayana, J. C. Dabrowiak and J. B. Chaires, *Biochemistry,* 1992, **31,** 9319–9324.

73. A.M. Polyanichko, V.V. Andrushchenko, E.V. Chikhirzhina, V. Vorobev and H. Wieser, *Nucleic Acids Res.,* 2004, **32,** 989–996.

74. V. I. Ivanov, L. E. Minchenkova, A. K. Schyolkina and A. I. Poletayev, *Biopolymers,* 1973, **12,** 89–110.

75. J. G. Collins, T. P. Shields and J. K. Barton, *J. Am. Chem. Soc.,* 1994, **116,** 9840–9846.

76. Q.-L. Zhang, J.-G. Liu, H. Chao, G.-Q. Xue and L.-N. Ji, *J. Inoorg. Biochem.,* 2001, **83,** 49–55.

77. M.T. Carter, M. Rodriguez and A.J. Bard, *J. Am. Chem. Soc.,* 1989, **111,** 8901–8911.

78. R.G. Parr and P.K. Chattaraj, *J. Am. Chem. Soc.,* 1991, **113,** 1854−1855.

79. P.V.R. Schleyer, C. Maerker, A. Dransfeld, H. Jiao and N.J.R.V.E Hommes, *J. Am. Chem. Soc.,* 1996, **118,** 6317–6318.

80. K.K. Bania and R.C. Deka, *J. Phys. Chem. C,* 2012, **116,** 14295–14310.

81. R. Rohs, I. Bloch, H. Sklenar and Z. Shakked, *Nucl. Acids Res.,* 2005, **33,** 7048–7057.

82. Y.G. Gao, A.H. Wang, *Anti-Cancer Drug Des.,* 1991, **6,** 137–149.

83. V. Kettmann, D. Kostalova and H.D. Holtje, *J. Comput. Aided Mol. Des.,* 2004, **18,** 785–797.

84. S. M. T. Shaikh, J. Seetharamappa, S. Ashoka and P. B. Kandagal, *Dyes Pigm.,* 2007, **73,** 211–216.

85. P. Sathyadevi, P. Krishnamoorthy, R.R. Butorac, A.H. Cowley, N.S.P. Bhuvanesh and N. Dharmaraj, *Dalton Trans.,* 2011, **40,** 9690–9702.

86. Y.-J. Hu, Y. Ou-Yang, C.-M. Dai, Y. Liu and X.-H. Xiao, *Bio macromolecules,* 2009, **11,** 106–112.

87. M. Anjomshoa, S.J. Fatemi, M. Torkzadeh-Mahani and H. Hadadzadeh, *Spectrochim. Acta Part A,* 2014, **127,** 511–520.

88. O.K. Abou-Zied and O.I.K. Al-Shihi, *J. Am. Chem. Soc.,* 2008, **130,** 10793–10801.

89. D.S. Raja, N.S.P. Bhuvanesh and K. Natarajan, *Dalt. Trans.,* 2012, **41,** 4365–4375.

90. M.T. Garland, J.Y. Le Marouille and E. Spodine, *Acta Crystallogr., Sect. C: Cryst. Struct. Commun.,* 1986, **42,** 1518–1520.

91. P. Krishnamoorthy, P. Sathyadevi, A. H. Cowley, R. Butorac and N. Dharmaraj, *Dalton Trans.,* 2012, **41,** 6842–6854.

92. J.R. Lakowicz, *Principles of Fluorescence Spectroscopy,* 2nd edn, Plenum Press, New York, 1999.

93. E. Gherardi and M. Stoker. *Nature,* 1990, **346,** 228–228.

94. C. Birchmeier and E. Gherardi, *Trends. Cell. Biol.,* 1998, **8,** 404–410.

95. C. Birchmeier, W. Birchmeier, E. Gherardi and G.F.V. Woude, *Nat. Rev. Mol. Cell. Biol.,* 2003, **4,** 915–925.

96. N. Inukai, T. Kawai and J. Yuasa, *Chem. Commun.,* 2011, **47,** 9128-9130.

97. N. Inukai, T. Kawai, and J. Yuasa, *Chem. –Eur. J.,* 2013, **19,** 5938–5947.

98. L. Huang and T. Kim, *Biol. Med.,* 2004, **37,** 735–736.

99. J.A. Hamilton, S. Era, S.P. Bhamidipati and R.G. Reed, *Proc. Natl. Acad. Sci. U.S.A.,* 1991, **88,** 2051–2054.

100. I.H. Goldberg, Molecular Aspects of Anticancer Drug-DNA Interactions; S. Neidle and M. Waring, CRC Press, Boca Raton, FL, 1993, vol. **1**, p. 243.

101. S. Goldstein and G. Czapski, *J. Am. Chem. Soc.,* 1986, **108,** 2244–2250.

102. S. Roy, S. Saha, R. Majumdar, R.R. Dighe and A.R. Chakravarty, *Polyhedron,* 2010, **29,** 3251–3256.

103. U. Basu, I. Khan, D. Koley, S. Saha, P. Kondaiah and A.R. Chakravarty, *J. Inorg. Biochem.,* 2012, **116,** 77–87.

104. G. Hacker and S.A. Paschen, *Expert. Opin. Ther. Targets.,* 2007, **11,** 515–526.

105. E. White, *Genes Dev.,* 1996, **10,** 1–15.

Targeting of DNA molecules, BSA/*c*-Met tyrosine kinase receptor and anti-proliferative activity of bis(terpyridine)copper(II) complexes

Dharmasivam Mahendiran[a], Raju Senthil Kumar[b], Vijayan Viswanathan[c], Devadasan Velmurugan[c] and Aziz Kalilur Rahiman[*a]

[a]*Post-Graduate and Research Department of Chemistry, The New College (Autonomous), Chennai 600 014, India.*

[b]*Department of Pharmaceutical Chemistry, Swami Vivekanandha College of Pharmacy, Elayampalayam, Tiruchengodu 637 205, India.*

[c]*CAS in Crystallography and Biophysics, University of Madras, Guindy Campus, Chennai 600 025, India.*

Table of Contents

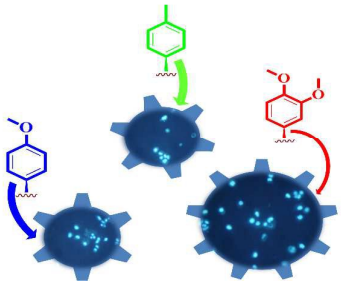

Highlights

The newly synthesized bis(terpyridine)copper(II) complexes may act as DNA-targeted metallo-anticancer agents to overcome cisplatin resistance.